JUACEP Summer Program 2019 at Nagoya University

Japan-US-Canada Advanced Collaborative Education Program

Nagoya University

Table of Contents

<1> About the Program

(a) Overview

Summer 10-week course 2019 for the students of University of Michigan and University of California, Los Angeles

Duration: June 18 – August 30, 2019
Research presentations: The 25th JUACEP Workshop on August 30, 2019

This program is designed for graduate students of the partner universities in US and Canada, and four students from University of Michigan and UCLA participated in 2019.

Each participant chose a research laboratory at Nagoya University in accordance with his/her research interest and carried out a research project under the supervisor of the laboratory. Japanese language class for beginner, the hands-on engine-model assembly course and some special events were organized for the program.

During the program period, they took part in the labs' activities such as seminars, sessions, trips, casual parties, and so on. Teaching Assistants (TA) assigned by the program supported the participants not only in research scenes but also in daily life.

At the end of the program, they submitted the research report to each supervisor and gave the final presentation at the 25th JUACEP Workshop, which took place at NIC Idea Stoa on August 30. Based on the evaluation of the report and presentation by each supervisor, the participants were accredited 2-3 units by Nagoya University. For the students at University of Michigan, those are admitted as graduation credits.

All participants with some advisors at the 25th Workshop on August 30, 2019

(b) Participants

	Name	Adviser & Teaching Assistant at NU
1	**Benye Tang** Mechanical Engineering Univ. Michigan	Prof. Noritsugu Umehara TA: Ruixi Zhang Micro-Nano Mechanical Science and Engineering
2	**Chen-Yu Cheng** Mechanical Engineering Univ. Michigan	Assoc. Prof. Shogo Okamoto TA: Yumena Iki Mechanical Systems Engineering
3	**Guanru Feng** Mechanical Engineering Univ. Michigan	Prof. Hosei Nagano TA: Yuki Akizuki Mechanical Systems Engineering
4	**Yu-Ching Hsiao** Mechanical Engineering UCLA	Prof. Satoshi Iwada TA: Wangzhen Zhao Electrical Engineering

Japanese Course Instructor

Ms. Sumie Yasui

Coordinators of Partner Universities

Prof. Katsuo Kurabayashi
Mechanical Engineering, University of Michigan

Prof. Jenn-Ming Yang
Materials Science and Engineering, UCLA

JUACEP Members

Prof. Yang Ju
Micro-Nano Mechanical Science and Engineering

Prof. Noritsugu Umehara
Micro-Nano Mechanical Science and Engineering

Prof. Toshiro Matsumoto
Mechanical Systems Engineering

Assoc. Prof. Yasumasa Ito
Mechanical Systems Engineering

Assoc. Prof. Takayuki Tokoroyama
Micro-Nano Mechanical Science and Engineering

Tomoko Kato
Administrative staff

(c) JUACEP Summer Program 2019 Schedule

Day	Date		8:45-10:15	10:30-12:00		13:00-14:30	14:45-16:15	16:30-
1	June 17	Mon	Check-in at International Residence Yamate South					
2	June 18	Tue	10:20 Reception - Orientation @ES Hall		Lunch	13:00 Stipend @Acct office	Lab introduction @each lab	
3	June 19	Wed	9:30-12:00 Jp Class① @Seminar-B, Library			Research @each lab		
4	June 20	Thu	Research @each lab					
5	June 21	Fri						
6	June 22	Sat						
7	June 23	Sun						
8	June 24	Mon	Research @each lab			Research @each lab		
9	June 25	Tue				13:45-16:15 Jp Class② @Seminar-B, Library		
10	June 26	Wed	9:30-12:00 Jp Class③ @Seminar-B, Library			Research @each lab		
11	June 27	Thu	Research @each lab					
12	June 28	Fri						
13	June 29	Sat						
14	June 30	Sun						
15	July 1	Mon	Research @each lab			Research @each lab		
16	July 2	Tue				13:45-16:15 Jp Class④ @Seminar-B, Library		
17	July 3	Wed	9:30-12:00 Jp Class⑤ @Seminar-B, Library			13:00 Stipend @Acct office	Research @each lab	
18	July 4	Thu	Research @each lab			13:00 Hands-on @IB-N, Creation Plaza, 10F		
19	July 5	Fri	Excursion, Meeting at Toyota Auditorium at 9:00am					
20	July 6	Sat						
21	July 7	Sun						
22	July 8	Mon	Research @each lab			Research @each lab		
23	July 9	Tue				13:45-16:15 Jp Class⑥ @Seminar-B, Library	Meet-up @347, EB-2	
24	July 10	Wed	9:30-12:00 Jp Class⑦ @Seminar-B, Library			Research @each lab		
25	July 11	Thu	Research @each lab					
26	July 12	Fri						
27	July 13	Sat						
28	July 14	Sun						
29	July 15	Mon	(Marine day)					
30	July 16	Tue	Research @each lab			13:45-16:15 Jp Class⑧ @Seminar-B, Library		
31	July 17	Wed	9:30-12:00 Jp Class⑨ @Seminar-B, Library			Research @each lab		
32	July 18	Thu	Research @each lab					
33	July 19	Fri						
34	July 20	Sat						
35	July 21	Sun						
36	July 22	Mon	Research @each lab			Research @each lab		
37	July 23	Tue				13:45-16:15 Jp Class Final @Seminar-B, Library		
38	July 24	Wed				Research @each lab		
39	July 25	Thu						
40	July 26	Fri						
41	July 27	Sat						
42	July 28	Sun						
43	July 29	Mon	Research @each lab			Research @ each Lab		
44	July 30	Tue						
45	July 31	Wed						
46	Aug 1	Thu						
47	Aug 2	Fri				13:00 Stipend @Acct office	Research @each lab	
48	Aug 3	Sat						
49	Aug 4	Sun						
50	Aug 5	Mon	Research @each lab			Research @each lab		
51	Aug 6	Tue						
52	Aug 7	Wed						
53	Aug 8	Thu						
54	Aug 9	Fri						
55	Aug 10	Sat	(Bon Holidays)					
56	Aug 11	Sun						
57	Aug 12	Mon						
58	Aug 13	Tue						
59	Aug 14	Wed						
60	Aug 15	Thu	Research @each lab			Research @each lab		
61	Aug 16	Fri						
62	Aug 17	Sat						
63	Aug 18	Sun						
64	Aug 19	Mon	Research @each lab			Research@each lab		
65	Aug 20	Tue						
66	Aug 21	Wed						
67	Aug 22	Thu						
68	Aug 23	Fri						
69	Aug 24	Sat						
70	Aug 25	Sun						
71	Aug 26	Mon	Research @each lab			Research @each lab		
72	Aug 27	Tue						
73	Aug 28	Wed						
74	Aug 29	Thu						
75	Aug 30	Fri	25th Workshop @NIC Idea Stoa		Lunch	ajournment		
76	Aug 31	Sat	Departure from Residence Yamate					

JUACEP event	Japanese class	Stipend payment	Holiday

<2> Research Achievements

(a) Research Internship

Research Reports

(b) Presentations

FRICTION CONTROLLING METHOD WITH OPTIMAL SOLID LUBRICANT CONDITIONS

Benye Tang

Integrative System + Design Department, College of Engineering, University of Michigan
benye@umich.edu

Supervisor: Noritsugu Umehara, Motoyuki Murashima and Takayuki Tokoroyama

Department of Micro-Nano Mechanical Science and Engineering, Graduate School of Engineering, Nagoya University
ume@mech.nagoya-u.ac.jp

ABSTRACT

This report aims to find some supportive advice for the friction controlling method based on Genetic Algorithm. To find the controlling method of stable friction, several relations between amplitude of coefficient of friction and other factors, such as number of contact points, different contact points patterns, thickness of coating film and roughness are studied. It is obviously that the surface roughness is the most significant factor, which has an approximate linear relation with amplitude of friction coefficient.

Keywords: *Friction stabilization, Solid lubricant, Coefficient of friction, Friction controlling method*

1. INTRODUCTION

There are many moving parts in the mechanical system, and the friction and abrasion caused by this part seriously affect the lifespan of the machinery. Especially for the specific machines such as artificial satellites and wind turbines, the contact damage resulted by wear and friction can cause significant economic losses and catastrophic consequences. Therefore, the longevity of the friction components is required. It is reported that, during the movement of the mechanical parts, its friction surface can get damaged resulted by various factors such as foreign objects mixing, adhesion, wear and stress damage. Finally, that kind of damage can result in unstable friction. Therefore, it is necessary to create an active friction surface which can adapt itself according to the change of external factors to achieve stable friction.

Stable friction has been studied for many years and it has been successfully applied to be many engineering fields. The optimization effort in previous studies is mainly about surface design. Murashima et al. [1] have developed a curved morphing surface consisting of morphing diaphragms which controls friction actively. M. A. Chowdhury et al. [2] have studied the effect of amplitude of vibration on the coefficient of the friction. Several authors [3-5] observed that the reduction of friction force depends on roughness of the rubbing surfaces, relative motion, type of material, temperature, normal force, stick slip, relative humidity, lubricant and vibration. Previous researchers T. Yamada et al. [6] have developed a contact points controlling system based on GA. At first, the contact points controlling system monitors the abnormal value of friction coefficient and gives various possible contact points patterns as the first generation, then evaluates each pattern and makes crossover to next generation's patterns by Genetic Algorithm. Finally, it will give a series contact points patterns which can escape from partial damages by air cylinder and achieve stable friction. However, we do not know why the contact points pattern given by smart system can control friction effectively. Moreover, this controlling system needs a lot of time to do the calculation and prepare for the GA controlling.

In this research, we aim to further study friction control mechanism by contact position controlling. Moreover, we want to study the cause of the contact position patterns given by GA which can achieve stable friction and find the setting parameters for GA to make the controlling system more efficient. And we are also interested in the effect of this method under solid lubricant conditions (MoS_2 and Polytetrafluoroethylene known as PTFE). Hopefully, this optimized control method will enable optimize the controlling system by improving its control precision and computation speed and reduce the expensive maintenance cost of sliding parts.

2. EXPERIMENTS

2.1 Apparatus and Friction Pair

The friction experiments were conducted using the tribo-tester designed by Nagoya University, which is shown in Fig. 1.

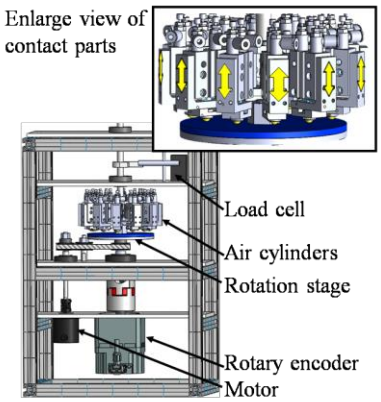

Fig.1 Tribo-tester

The Tribo-Tester consists of a rotation table and the contact points controlling system. The brushless motor (Orientalmotor Company) was used to rotate on a friction tester. The engine driver BLE2D120-a was used by which the motor speed can be controlled by external signals. In the experiment of this study, a software named LabVIEW is used to control the speed, start and stop of the motor. The contact points controlling system has 12 air cylinders which are evenly distributed by every 30° and can be controlled by compressed air independently in two directions up and down. Equipped with a beam load force sensor, the setup can monitor the friction force with electrical signals. The signal collecting device records the data in real-time and the sampling frequency is 10 Hz. The measurable friction force is the force generated by all the friction test machines consisting of 12 cylinders. The friction force generated at 12 contact points cannot be measured separately.

The disks are made of MC nylon and PTFE with a size of Φ130 × 5 mm. The contact point with a size of Φ8 mm is made of high-carbon chromium bearing steel (hereinafter referred to as SUJ2 balls). The surface roughness of SUJ2 ball after mirror treatment is Ra = 10 nm, and the hardness of HRC is about 60. The appearance of the SUJ2 balls used as a contact point is shown in Fig. 2.

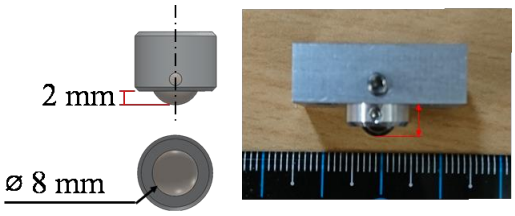

Fig. 2 Contact point (SUJ2 ball)

And in this experiment, we use 3D measuring laser microscope OLS5000 to measure the surface roughness.

2.2 Experimental Method

2.2.1 the effect of number of contact points

Since there are thousands of different contact points patterns, the symmetrical patterns with different numbers of contact points have been tested first. The patterns are shown in Fig. 3.

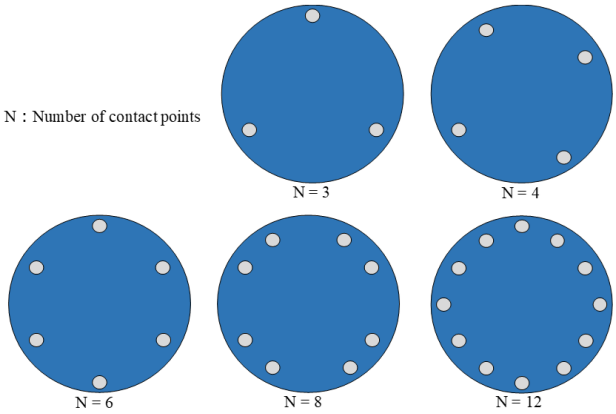

Fig. 3 Symmetrical patterns of different # contact points

To acquire similar roughness and uniform MoS_2 coating film, the Nylon plate was placed on the rotator machine which runs at a constant rotation speed. Then MoS_2 spray coated the plate from the same height (10 cm from Nylon plate) by 10 seconds. The process of coating is shown in Fig. 4.

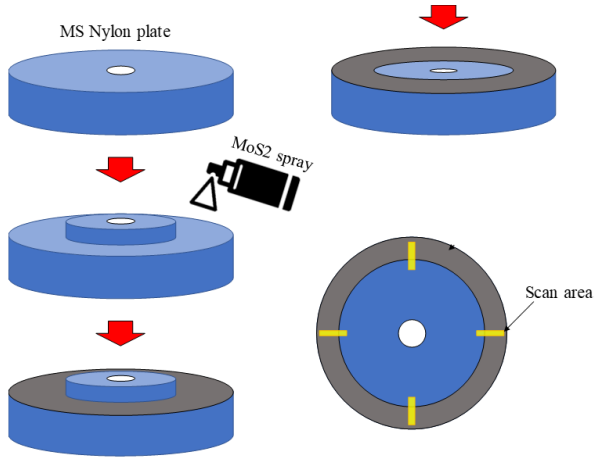

Fig.4 Coating process

The profiles of these plates have been scanned by OLS5000 to get initial roughness. Before conducting experiment, the contact points need to be cleaned with acetone by 15 min. Then the number of contact points is changed by GUI, which is shown in Fig. 5:

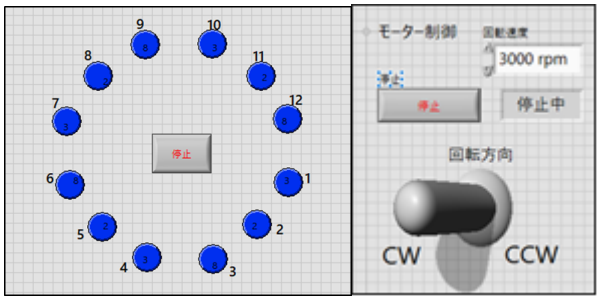

Fig.5 Graphical user interface

And then fix the plate on the tribo-tester, with a load of W = 13.4 N, a constant rotation speed of ν = 40 rpm, and the same test durations of 14400 seconds. Because the data is recorded by electrical signals, it can be transferred to coefficient of friction by using the following formula:

$$\mu = \frac{F[N]}{W[N]} \quad (1)$$

$$F = \alpha|V| \quad (2)$$

$$\mu = \frac{\alpha|V|}{W[N]} \quad (3)$$

α : Load cell device const.

$|V|$: Absolute value of measured voltage value, V

W: Normal load, N (W = 13.4 N)

F: Friction force, N

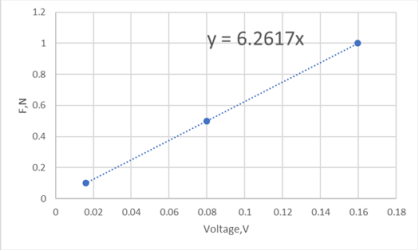

N	V
0.1	0.01597
0.5	0.079851
1	0.159701

Fig. 6 Load cell device constant

This Fig. 6 shows that relation between load[N] and voltage[V]. It gives load cell device constant α = 6.2617, and then the measured voltage can be transferred to friction coefficient.

The friction tests with the same experiment conditions have been conducted on PTFE plates without MoS_2 coating, also, to compare the effect of different solid lubricant materials.

2.2.2 the effect of unsymmetrical patterns

Considering the principle of Genetic Algorithm, some 'bad' generations should not be dropped, because some of them may have recessive advantages. The pattern of 6 contact points was chosen, generating 4 unsymmetrical patterns, which are shown in Fig. 7. These experiments had been conducted under the same experimental conditions as previous ones.

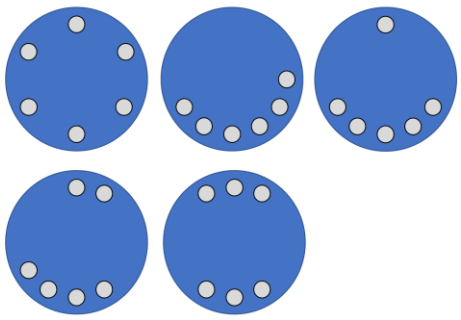

Fig. 7 Unsymmetrical patterns

2.2.3 the effect of the thickness of coating film

The friction tests with different thickness of coating film under same experimental conditions have been conducted either. The MC nylon plates were coated using the same coating process, but different spray time by 10 seconds, 30 seconds and 60 seconds. To compare to other experiments easily, the 6 contact points symmetrical pattern was chosen again. And the initial height of each MoS_2 coating film and the depth of wear tracks were measured by OLS5000.

3. RESULTS AND DISCUSSIONS

3.1 The effect of numbers of contact points

In this section, the influences of different number of contact points and performances of 2 different kinds of solid lubricant materials are specifically discussed.5 different number of contact points symmetrical patterns (#3, #4, #6, #8 and #12), and 2 different kinds of solid lubricant materials (MoS_2 and PTFE) were involved in this section.

This report aims to find the best controlling method to get the stable friction. The amplitude of the friction coefficient is the important factor which reflects that it is stable friction or not. The amplitude of coefficient of friction (CoF) was calculated in each cycle by using the following formula:

$$\text{Amplitude of CoF} = \text{CoF}_{max} - \text{CoF}_{min} \quad (4)$$

During the 14400 seconds of friction test, the plate runs at 40 rpm, then every 1.5 seconds it runs one cycle. And the sampling frequency is 10 Hz, then 15 data of CoF was collected in one cycle. It is easily to find the maximum and minimum CoF in 15 records and get the amplitude of CoF, marked as ΔCoF.

Figure 8(a) and 8(b) plot the amplitude of coefficient of friction on different symmetrical patterns with cycles. In Fig. 8(a) and 8(b), the patterns of #6 and #8 show better performance, lower fluctuation of amplitude of friction coefficient on both two different kinds of solid lubricant materials, MoS_2 and PTFE.

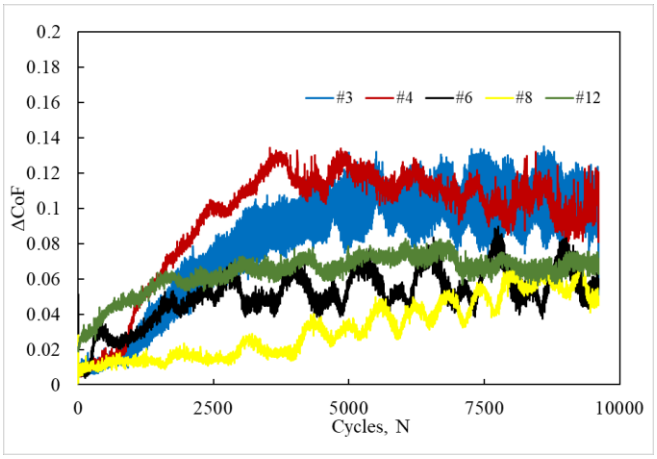

Fig. 8(a) ΔCoF – Cycles on MoS_2

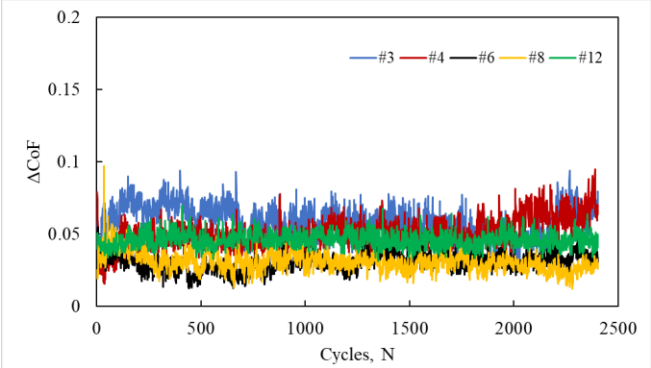

Fig. 8(b) ΔCoF – Cycles on PTFE

Since almost all of the friction tests have running-in process, further study focuses on the last 100 seconds of friction test. Fig. 9(a) and 9(b) plot the average of the amplitude of the coefficient of friction in the last 100 seconds with the roughness of after-test on each plate. In both Fig. 9(a) and 9(b), the ΔCoF_{avg} almost has the linear relation with Ra, which means the roughness is very significant factor which can affect the amplitude vibration of friction coefficient. It also means the lower the surface roughness, the more stable the friction.

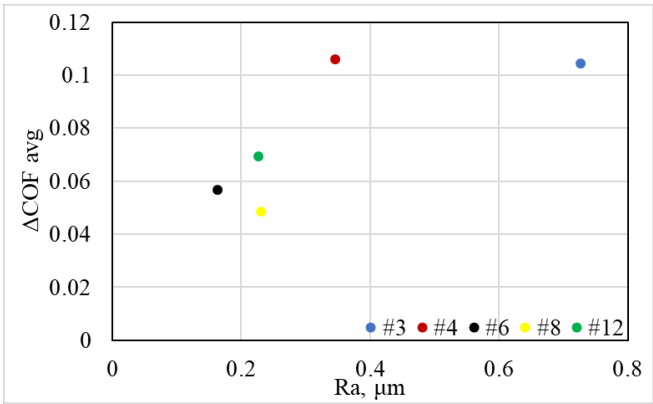

Fig. 9(a) ΔCoF_{avg} – Ra on MoS_2

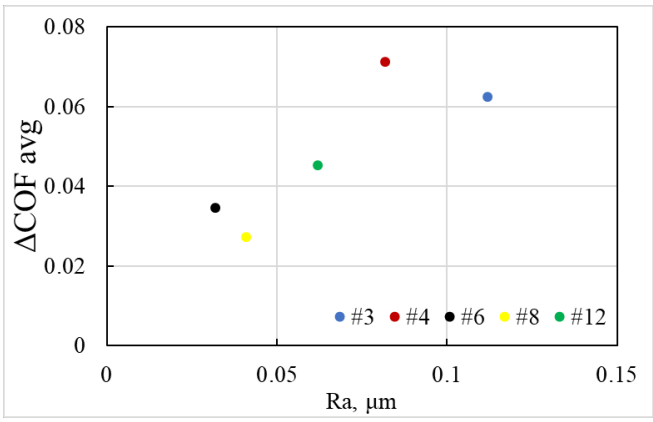

Fig. 9(b) ΔCoF_{avg} – Ra on PTFE

From Fig.8 and Fig. 9, the patterns of #6 and #8 showed the much better performances than the patterns of #3 and #4. The after-experiment surface profiles of MoS_2 coating film were scanned by OLS5000, which are shown in Fig. 10(a), 10(b), 10(c), 10(d) and 10(e). Because of the pressure of patterns #3 and #4 is much higher than that of patterns #6, #8 and #12, a lot of cracks and the obvious peeling-off MoS_2 coating films are shown in Fig. 10(a) and 10(b). While in the Fig. 10(c), 10(d) and 10(e), the surfaces are relative smooth with fewer cracks.

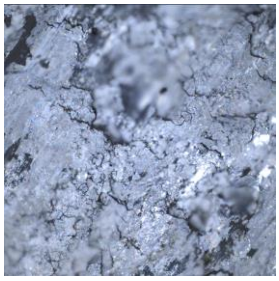

Fig. 10(a) #3

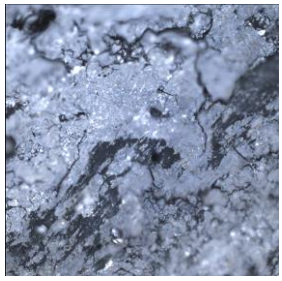

Fig. 10(b) #4

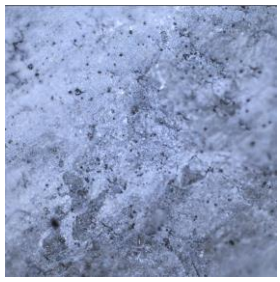

Fig. 10(c) #6

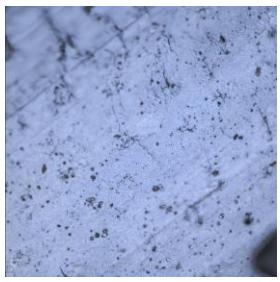

Fig. 10(d) #8

Fig. 10(e) #12

3.2 The effect of unsymmetrical patterns

In this section, different patterns including Centro symmetrical patterns (#6), Reflection symmetrical pattern (#3,3) and unsymmetrical patterns (#6,0 #5,1 and #4,2)are discussed.

From Fig. 11, the symmetrical pattern #6 shows the best performance, with lowest amplitude of friction coefficient. And the reflection symmetrical pattern #3,3 shows the good performance too. Even though its amplitude of friction coefficient is a little bit high, its rate of change is almost constant. While the unsymmetrical patterns #6,0 #5,1 and #4,2, have the much bigger amplitude of friction coefficient, which means the plates were tested under very unstable friction. Then, this assessment confirms that

symmetrical patterns have the advantage over other unsymmetrical patterns.

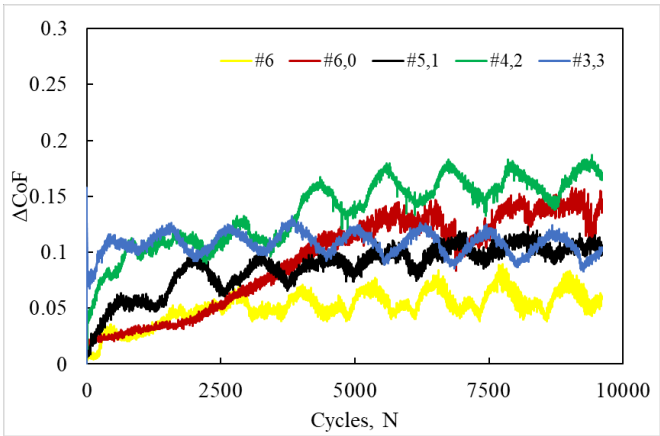

Fig. 11 Unsymmetrical patterns

3.3 The effect of the thickness of coating film

In this section, the relation between surface roughness and amplitude of friction coefficient is discussed. In Fig. 12, there is an obvious linear relation between surface roughness Ra and amplitude of friction coefficient, which confirms the surface roughness is a significant factor again.

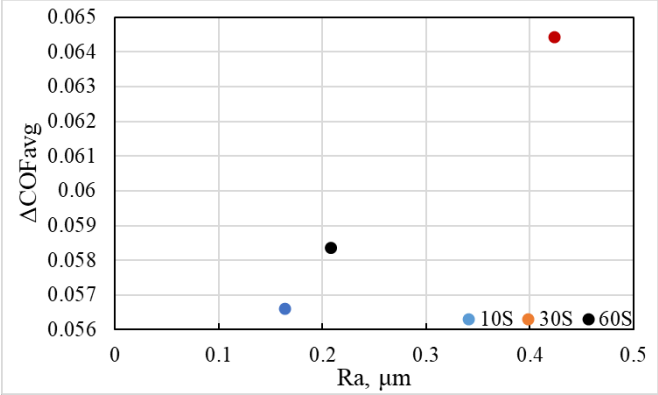

Fig. 12 ΔCOF_{avg} – Ra with different thickness

Except that, the thickness of coating films and the depth of wear tracks are measured by OLS5000, which are shown in the following Table 1.

Table 1 The different thickness of coating films

spray time(sec)	Film thickness(μm)	Wear track depth(μm)	Remained thickness(μm)
10s	54.9	25.4	29.5
30s	94.8	56.5	38.3
60s	130	118	12.3

Even though, the plate with 60 seconds MoS_2 spray has the thickest coating film, its wear track is the deepest, reaming the least MoS_2 film. And the plate with 30 seconds MoS_2 spray which shows the highest surface roughness in Fig. 12, has the most remaining MoS_2 film. Moreover, the plate with 10 seconds MoS_2 spray shows the best performance, even its initial film is thin. In this case, maybe because of the thicker the MoS2 coating film, the softer. And that means it is easy to be worn out.

4. CONCLUSIONS

In this research work, the effect of different number of contact points, roughness, different contact position patterns and thickness of coating film are discussed. Patterns with #6 and #8 contact points showed the best performance, while the patterns with #3 and #4 had the bigger amplitude of friction coefficient. Therefore, the patterns with a greater number of contact points are recommended. And the patterns with fewer number of contact points have the bigger pressure which will result in the cracks on the friction surface and higher surface roughness. Therefore, when applied with the Genetic Algorithm controlling method under solid lubricant conditions, the fewer contact points which equals to higher contact pressure should be carefully considered.

Also, several experiments' results show that roughness has an almost linear relation with amplitude of friction coefficient. In the future research, the study of surface roughness needs to be attached importance. And the assessment confirms that the symmetrical patterns have the advantage over the unsymmetrical patterns.

Moreover, the effect of thickness of coating film needs to be further studied, to find the best thickness.

ACKNOWLEDGEMENTS

Thanks to JUACEP program for providing such a great opportunity for me to conduct academic research. I spent a wonderful summer vocation in Nagoya University. Thanks to Umehara Lab, Umehara Sensei, Murashima Sensei, Tokoroyama Sensei, Yamada San and other lab members for helping me a lot during the research.

REFERENCES

[1] M. Murashima, et al, "Intelligent tribological surfaces: from concept to realization using additive manufacturing" International Journal of Mechanics and Materials in Design, (2019): 1-10.
[2] Chowdhury, Mohammad & Maksud Helali, Md. (2008). The effect of amplitude of vibration on the coefficient of friction for different materials. Tribology International. 41. 307-314. 10.1016/j.triboint.2007.08.005.
[3] Archard, J. (1980). Theory and mechanisms of wear. Wear Control Handbook.
[4] Tabor, D. (1982). Friction and wear. Tribology International. 15. 10.1016/0301-679x(82)90085-8.
[5] J. Berger, E & Krousgrill, Charles & Sadeghi, Farshid. (1997). Stability of Sliding in a System Excited by a Rough Moving Surface. Journal of Tribology-transactions of The Asme - J TRIBOL-TRANS ASME. 119. 10.1115/1.2833868
[6] T. Yamada, et al, "Development of Control Method for Friction Stabilization".

APPENDIX

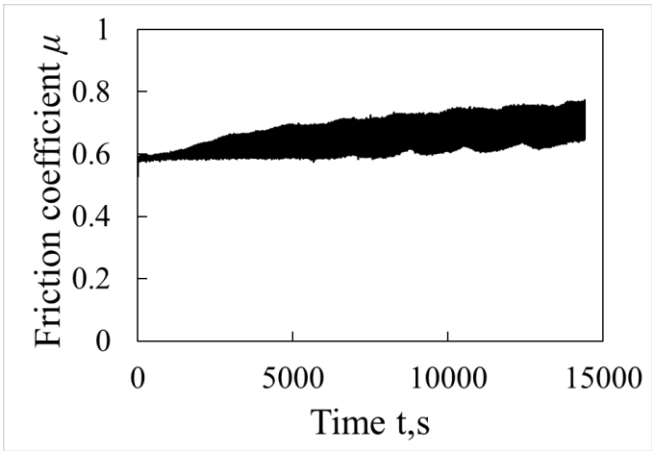

Fig.1 Pattern #3

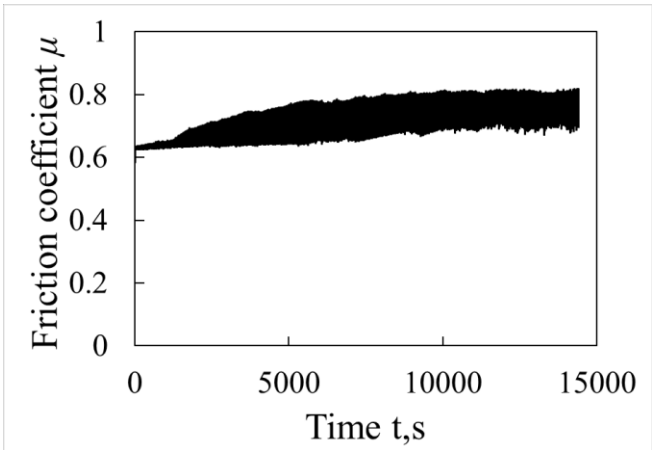

Fig.2 Pattern #4

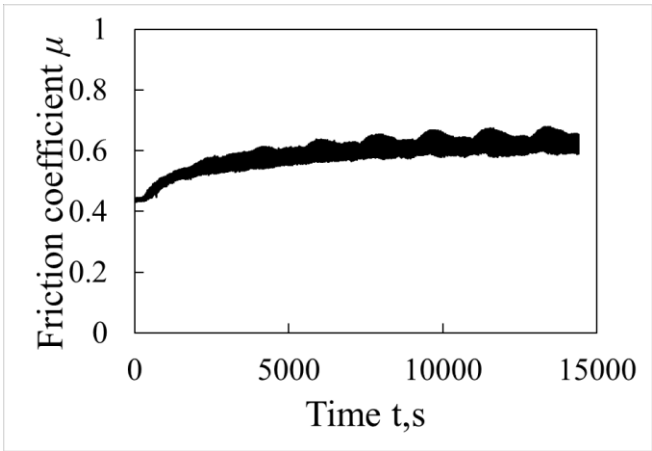

Fig.3 Pattern #6

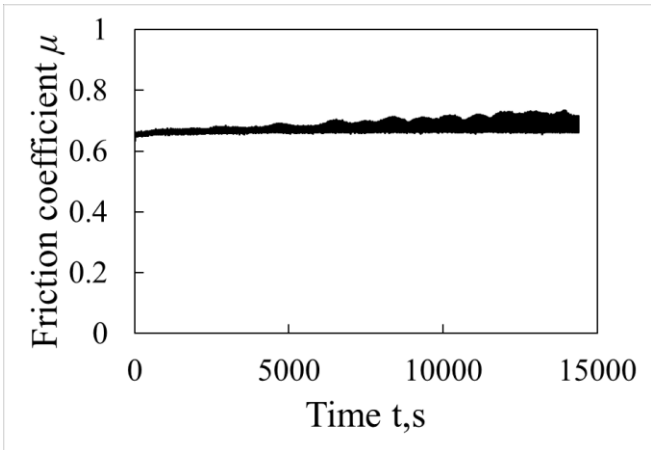

Fig.4 Pattern #8

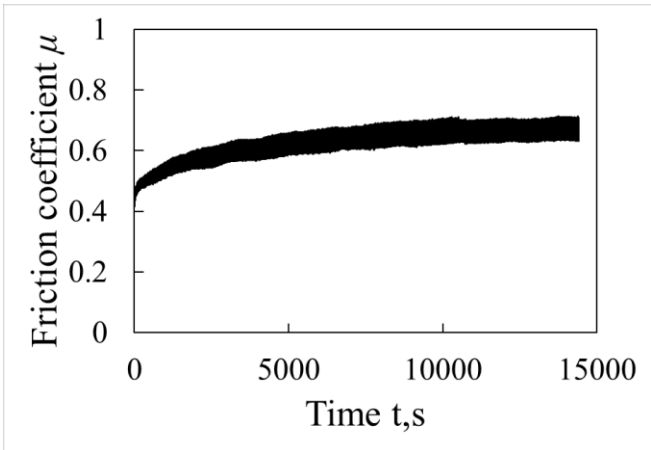

Fig.5 Pattern #12

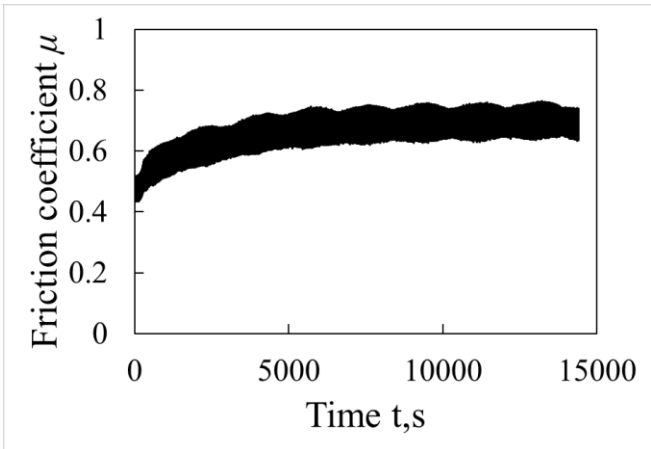

Fig.6 Pattern 3,3

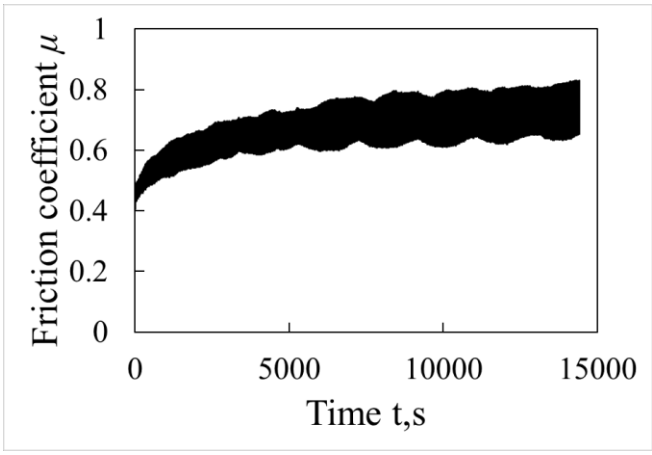

Fig.7 Pattern 4,2

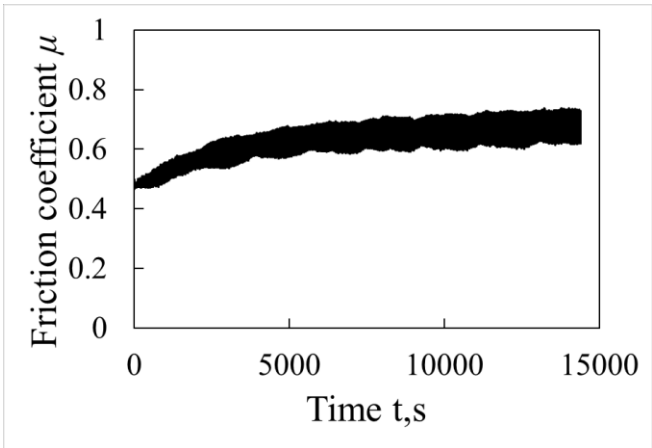

Fig.8 Pattern 5,1

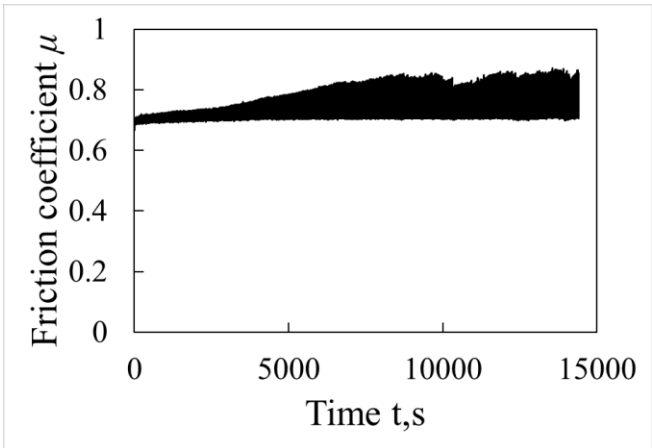

Fig.9 Pattern 6.0

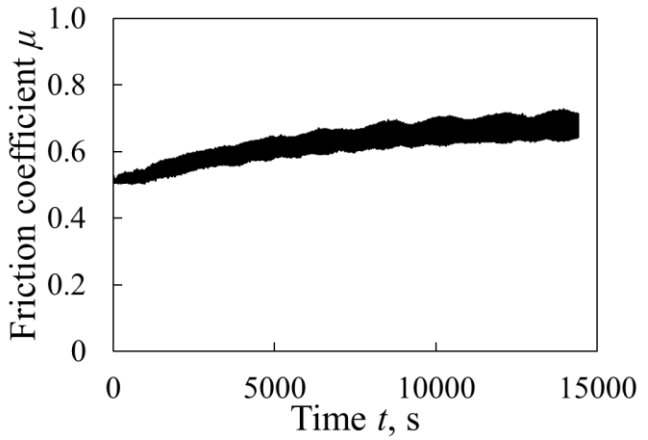

Fig.10 Pattern 30s

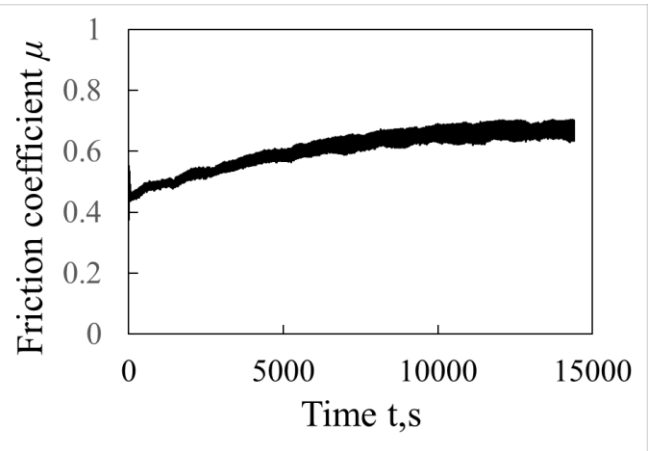

Fig.11 Pattern 60s

ENCOURAGEMENT OF SQUAT-LIFTING: FEASIBILITY STUDY OF A HIGHLY USABLE PASSIVE KNEE ASSISTIVE DEVICE

Chen-Yu Cheng

Department of Mechanical Engineering, University of Michigan
cchenyu@umich.edu

Shogo Okamoto

Graduate School of Engineering, Nagoya University
Okamoto-shogo@mech.nagoya-u.ac.jp

ABSTRACT

Low back pain (LBP) is a serious occupational disease. A main contributing factor to LBP is lifting heavy objects. To reduce the risk of LBP, squat-lifting, which uses knee torque, is recommended as a preferred alternative to stoop-lifting, which uses back muscles more. However, people tend to avoid squat-lifting due to its relatively low metabolic efficiency, and the greater force it places on the knee and rectus femoris. Many lifting assistive devices have already been commercialized to cope with LBP. However, the majority are designed to support back or hip muscles, not to encourage workers to perform squat-lifting. Therefore, we fabricated a prototype knee assistive device that is easy-to-wear and light-weight, using shape-memory-alloy (SMA) wires that are inherently passive elements. We then tested the effectiveness of the device by measuring electromyography (EMG) levels in the rectus femoris during squat. At knee bending positions, the device reduced EMG levels in the rectus femoris by at least 15% on average.

1. INTRODUCTION

Multiple original studies [1], [2], [3] and systematic reviews [4], [5] agree that manual lifting is a major cause of developing low back pain (LBP). When lifting heavy objects, two predominant methods are stoop-lifting and squat-lifting, as shown in Fig. 1. Squat-lifting relies on knee torque for lifting, while keeping the torques from the back low. Stoop-lifting is characterized by an inclined trunk and almost fully extended knees. In one definition, the postural index, which is the ratio between knee flexion from normal standing and the sum of ankle, hip, and lumbar vertebral flexions from normal standing, is approximately 0.80 for squat-lifting and 0.11 for stoop-lifting [6]. Squat-lifting reduces the maximum voluntary contraction in the erector spinae compared to stoop-lifting [7], and the shear forces applied to lumbar for stoop-lifting are estimated to be 180% greater than squat-lifting [8]. Furthermore, stoop-lifting is reported to have caused approximately 75% more stresses on discs and ligaments than squat-lifting [9]. Consequently, the governmental ministry in Japan recommends squat-lifting to lower the risks of LBP [10]. However, squat-lifting is 23% to 34% less metabolically efficient than stoop-lifting [11]. The maximum oxygen consumption during squat-lifting is 14.3% more than that during stoop-lifting [12], and the maximum heart rate during squat-lifting is 6.5% more than that during stoop-lifting [12]. Furthermore, squat-lifting increases maximum muscle contraction in the rectus femoris [7]. As a result, although squat-lifting can be effective in preventing LBP because it exerts less shear stress on lumbar discs, it is more fatiguing and thus, less frequently used.

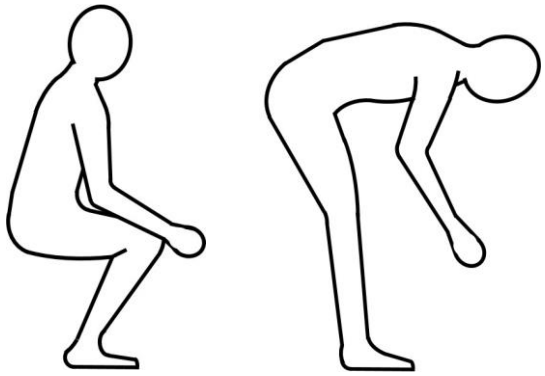

Fig. 1: Schematic diagrams of squat-lifting (left) and stoop-lifting (right)

To prevent or manage LBP, several wearable assistive devices have been developed and commercialized in recent years. The majority of these devices provide external support to the lumbar spinae when lifting objects. Depending on how external forces are applied, there are two types of assistive devices: active and passive. Active devices use actuators such as electromagnetic, electrohydraulic, and electropneumatic to generate the external forces; passive devices use intrinsically passive elements to store energy during negative works, and then release the stored energy during positive works.

Fig. 2: Knee assistive device built on a commercial knee supporter with shape-memory-alloy wires

Hybrid Assistive Limb (Cyberdyne, Ibaraki, Japan) [13], [14] and Mk2b [15], [16], a revised version of Robo-Mate [17], are examples of active assistive devices with two electromagnetic motors on the hip joints of the wearer. Both devices provide assistive torque to wearers' hip and trunk to support the lifting motion. In contrast, the Laevo (Laveo,The Netherlands) [18] is a passive assistive device that uses pads contacting wearers' chest, back, and upper legs, and a circular tube with spring-like characteristics that connects these pads to generate upward forces to the chest; the reactive forces are supported by the wearers' legs. A garment-like device [19], designed by Vanderbilt University, USA, is another passive device that uses elastic bands to provide extension momentum to the lumbar. Additional devices have been either commercialized or in development.

These assistive devices have trade-offs between effectiveness and usability. The active ones produce more effective support, but some require external energy sources and are heavier. The wearability is not high because these devices use rigid links and cuffs and allow limited degrees of freedom during use. The passive devices, on the contrary, are light-weight and are more practical to use when wearers need to move around frequently and in circumstances where external power sources are not available.

Assistive devices can also be categorized by supported area. Assistive devices for lifting are focused on protecting the lower back and hips. Other assistive devices provide support to the knees or ankles and can be utilized for walking assistance [20], [21], [22], [23], [24]. However, giving support to the lower back and hip joints does not change the wearers' behavior from stoop-lifting to squat-lifting. Consequently, we focused on a knee assistive device to encourage laborers to conduct squat-lifting to lower the risk of LBP.

To expand the use of squat-lifting, this study aims to develop a knee assistive device with high usability by using shape-memory-alloy (SMA) wires as passive elements. This device takes advantage of the superelastic property of SMA to provide external forces to the rectus femoris, encouraging workers to perform squat-lifting by compensating for the part of the necessary knee torque. In this paper, we describe the designing process and policies of the device and evaluate the effectiveness of the device experimentally by measuring the electromyography (EMG) of the rectus femoris.

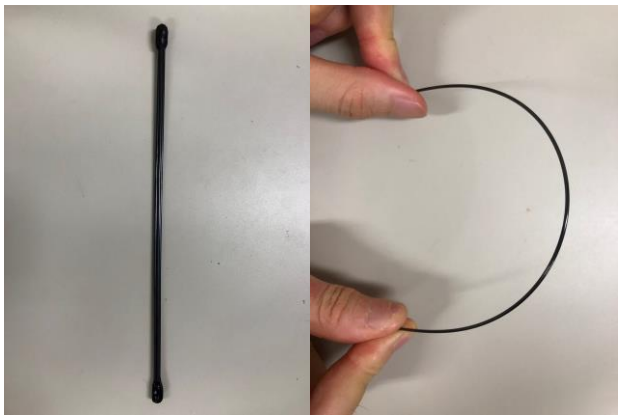

Fig. 3: The left panel is a single strand of the SMA wire. Thermoplastic resin was applied on the two ends of four wires to bind them together. The right panel shows a SMA wire under bending conditions.

2. KNEE ASSISTIVE DEVICE

The knee assistive device consists of two main parts: a cloth knee brace and SMA wires. The knee brace functions as a splint on which to install the SMA wires, while the SMA wires provide the external forces to support rectus femoris. The ends and the middle part of the wires, which are the vertices during bending, are fixed to the knee brace. This design positions the bending center of each wire at the rotational center of the knee on the sagittal plane. The device is shown in Fig. 2.

2.1 KNEE BRACE

A commercial hinged knee brace (54557, Mueller Sports Medicine Company, Germany) was chosen to be part of the assistive device. The hinges of the knee brace, which are used to prevent the medial-lateral motion of the knee to protect damaged knees, were removed. Therefore, the brace was used as a soft chassis on which to attach the SMA wires to provide supportive force while bending.

The brace is designed to be easy-to-wear by using two Velcro strips, which allow the wearer to put on and off the device without needing to remove his or her shoes.

2.2 SHAPE-MEMORY-ALLOY WIRES

The SMA wires are made of nickel-titanium (Ni-Ti) alloy (Yoshimi Inc., Japan). Supportive forces are generated by the superelasticity property of SMA, which is more accurately described as pseudoelasticity. As shown in Fig. 3, four wires were joined together with thermoplastic resin. Each strand of wires was put in a pocket at each side of the knee brace, thus there were a total of eight SMA wires per knee. The maximum knee torque for sit-to-stand movement is 0.38 Nm/kg for normal people [25]. Thus, for a 70-kg person, it requires 26.6 Nm to perform sit-to-stand

movements. The number, length, and diameter of the SMA wires were selected to produce 10% of the required torque. This value (10%) was chosen so that the device would reduce the intensity of muscle activity required during the sit-to-stand motion without the wearer feeling a resistive force during the other activities, which would be perceived as a nuisance. The choice was subjective because, to the best of our knowledge, such a minimum resistive force that does not subjectively or physically disturb the motion of wearers has yet to be determined. Therefore, no current literature or data is available to determine an optimal percentage for the level of support provided by passive knee assistive devices. Furthermore, our device was designed to generate 10% of the necessary torques when the wearer is not lifting any additional weight. It should be noted that the support ratio of the device will be smaller than 10% while lifting additional weight. The performance tests we used to determine the values of the length, diameter, and the number of wires will be described in the next subsection.

2.3 DETERMINATION OF THE LENGTH AND DIAMETER OF SMA WIRES

We conducted experiments to determine the optimal length and diameter of SMA wires in terms of the forces generated by the wires. A push-pull scale (FB-100N, Imada Co. Ltd., Japan) was used to measure the restoring force when the wire was bent at set angles. One end of the SMA wire was fixed to the push-pull scale, and an external force was applied to the other end to bend the wire to a certain angle. The push-pull scale was aligned with the direction of the restoring force of the wire. The maximum knee angle of a sit-to-stand motion is approximately 100°. Therefore, the resultant torque was measured at 100°.

To experimentally evaluate the diameter, SMA wires having diameters of 1.0, 1.2, and 1.5 mm, and a common length of 20 cm were compared. Four wires of the same diameter were joined together for the measurements, and the results are shown in Fig. 4. SMA wires of larger diameter generated greater torques during bending. The relationship between diameter and torque was nonlinear and quadratic.

For the length test, the diameter of the SMA wires was fixed to 1.0 mm, and the length ranged from 16 cm to 34 cm with an interval of 2 cm. Different from the length test, we only used one wire to measure the forces for this test. As shown in Fig. 5, the shorter SMA wires exhibited higher torque, whereas the torque is not significantly different when the wire length is more than 20 cm. Nonetheless, when shorter wires are used, the clothing area that supports the wires is also smaller, and the restoring force damages the cloth material of the knee brace.

Based on these performance tests, we determined that the optimal length, diameter, and number of wires is 22 cm, 1.8 mm, and 8, respectively. To make these determinations, inter- and extrapolation of the data were used. This combination achieves the supportive torque desired.

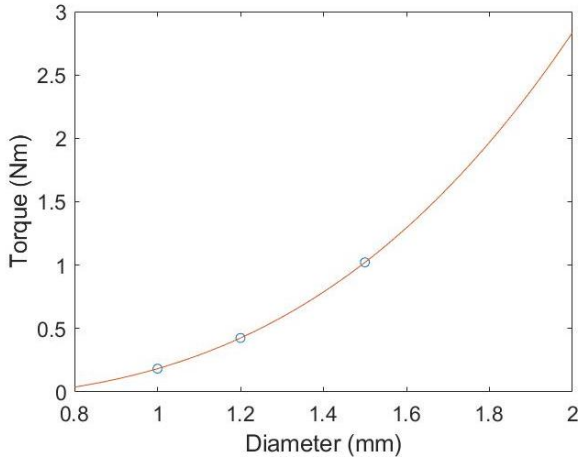

Fig. 4: The relationship between diameter and torque of SMA wires. All wires were 20 cm in length, and four wires of identical diameter were joined together. Torques were determined with the wires bent at 100°

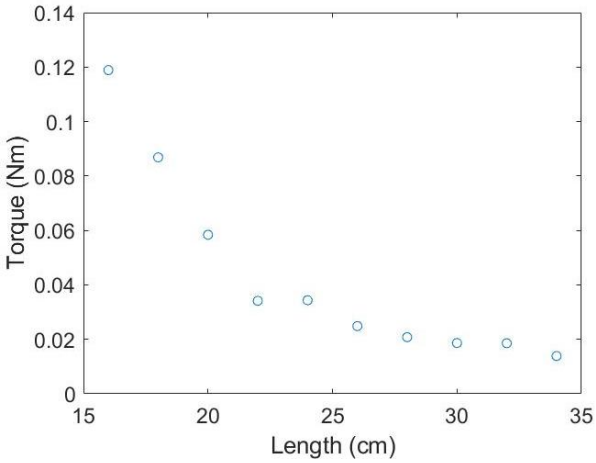

Fig. 5: The relationship between length and torque of SMA wires. The diameter of each wire was 1.0 mm. Torques were determined with the wires bent at 100°

3. EFFECTIVENESS TESTS

3.1 PARTICIPANTS

Three participants agree to test the EMG value while squatting. The average height and weight of the participants were 166.7 ± 9.1 cm and 55.3 ± 5.9 kg, respectively. All participants were healthy with no injuries or diseases.

3.2 EXPERIMENT PROCEDURES

We measured the EMG signals of the rectus femoris under four different conditions: 45° or 90°-squat with or without the knee assistive device. For each trial, the participants were asked to squat to the assigned angle, then pause at the position for five seconds. A constant height chair was used as a mark to let the participant know whether his or her knee angle was close to the designated value. This task mimicked a situation in which the participant was

expected to hold and lift an object by squat-lifting. To avoid accidental injuries, the participants did not have any actual loads in their hands. Each condition was repeated a total of 10 times by each participant. To avoid the effect of muscle fatigue, the four conditions were tested in randomized order with each condition repeated five times in succession.

3.3 DATA ANALYSIS

To process the EMG signals, we focused on the central three seconds within the five-seconds-pause to prevent the different speed of participants' squatting behaviors from affecting the results. We calculated the mean voltage signal of each trial, and then compared the difference between the trials done with and without the knee assistive device. Although we planned to exclude samples where the variation exceeded two standard deviations, there were no outliers among the samples. However, we did exclude some trials, in which the EMG signals were intermittent because of false skin-electrode contact as invalid.

3.4 RESULT

The mean EMG signals and the *p*-values of Welch's *t*-test of the three participants are shown in Fig. 6. There are significant differences between the conditions with and without the knee assistive device for both angles. For each of the three participants, the mean EMG signal decreased by 27.7%, 26.8%, and 52.1% when squatting 45°; and decreased by 14.7%, 22.9%, and 38.4% when squatting 90°. The effectiveness of the knee assistive device varies for each participant, which may be because the weight of each participant is different.

4. DESIGNING THE SMA WIRE FIXATION MECHANISM FOR OPTIMAL USABILITY

To increase usability, a mechanism for easily installing and uninstalling the SMA wires is proposed in Fig. 7. The mechanism consists of two parts. One part looks like a cylinder with two square holes, which is used to confine the horizontal movement of the wires. The other part is a lid with two ``ears" to confine the vertical movement of the wires. There are two convex squares on the ears that fit into the two square holes in the cylinder. The lid can be easily removed by pressing the ears. A detailed procedure of utilizing the mechanism is shown in Fig. 7b. With this mechanism, users can turn on and off the supportive torque without taking off the knee assistive device. The bottom end of the SMA strand is inserted into the pocket of the knee brace while the top is anchored by the mechanism. This mechanism has no effect on the assistive performance; however, it contributes to the usability of the assistive device.

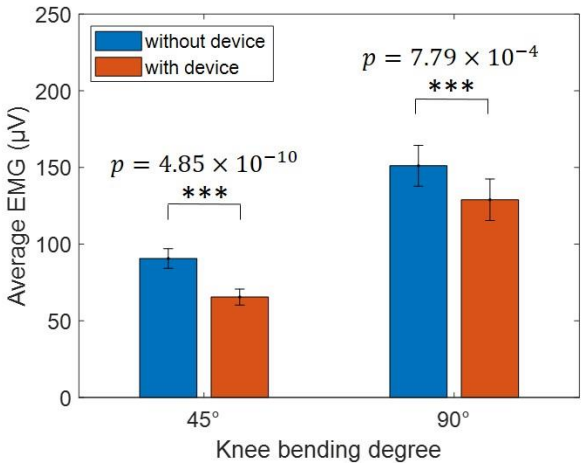

(a) Participant 1

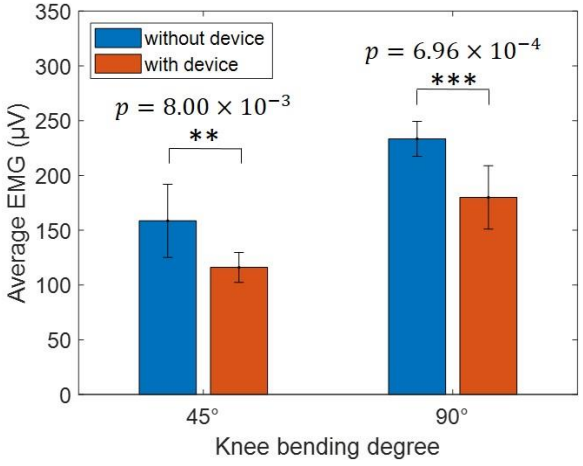

(b) Participant 2

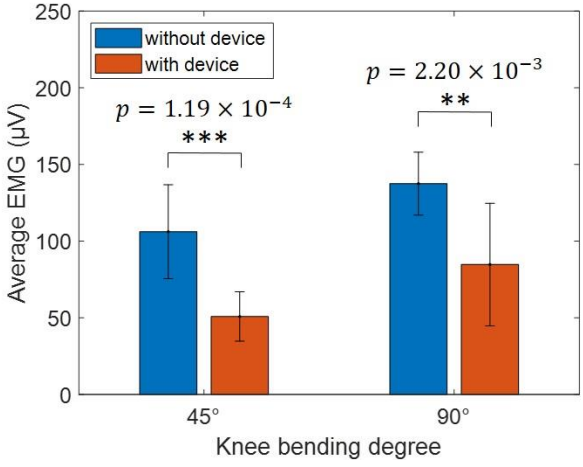

(c) Participant 3

Fig. 6: EMG values of the rectus femoris.**: p<0.01, ***: p<0.001

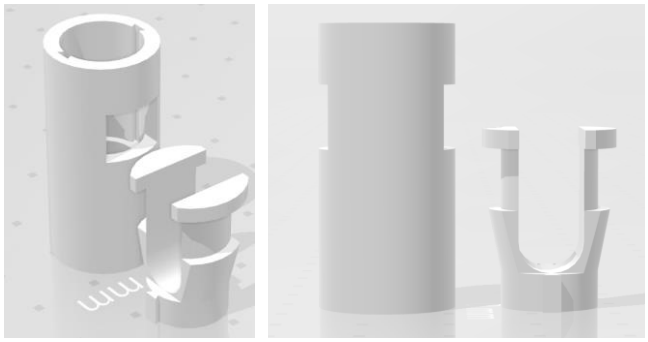

(a) CAD images of the fixation mechanism

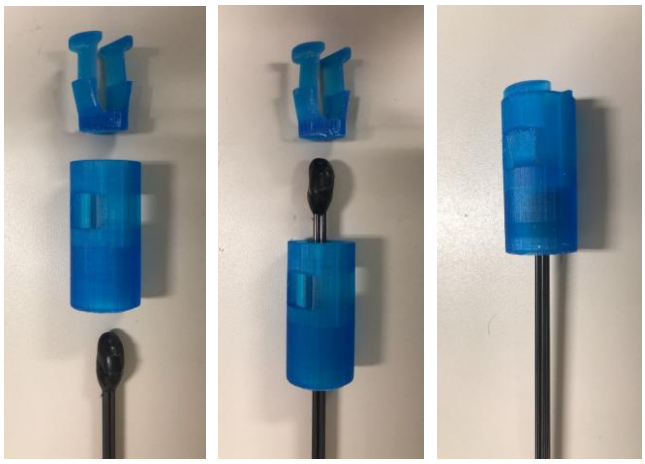

(b) Fixation mechanism manufactured by a three-dimensional printer. From left to right, the panels illustrate how to confine the SMA wires in the tube.

Fig. 7: Fixation mechanism

5. CONCLUSION

Many published reports and government agencies recommend using squat-lifting instead of stoop-lifting to reduce the risk of low back pain. To encourage people to perform squat-lifting, we made a prototype of a light-weight and easy-to-wear passive knee assistive device. This device consists of a commercial knee supporter and two strands of SMA wires. One device is worn on each knee. The SMA wires do not lose their elasticity even when they are bent at larger angles and generate restoring forces. A fixation mechanism for the SMA wires was devised to easily turn the assistive device on and off without taking off the knee brace. The device was designed to support approximately 10% of the maximum torques for healthy people weighting 70 kg to perform sit-to-stand movements. Four different conditions were compared experimentally evaluate the effectiveness of the prototype: squats at 45° and 90° with and without the assistive device. The EMG values of rectus femoris were collected while three participants performed each condition in a randomized order. The results indicate that, with the knee assistive device, the participants decreased the activity of the rectus femoris muscle by 14.7%—52.1%. The participants were lighter than 70 kg, so the observed effects were higher than expected. The proposed knee assistive encourages people to change their lifting behavior from stoop-lifting to squat-lifting. Nonetheless, further usability tests are needed to evaluate the practical utility of the proposed device and include subjective feedback from occupational users. Furthermore, although we did not use any loads in this study, if the participants had lifted actual weights, then the magnitude of reduction of the EMG signals during use of the assistive device would have been lower.

ACKNOWLEDGEMENTS

I would gratefully thank Prof. Okamoto for giving me opportunity to do research in Nagoya University, and providing me guidance through this project. Also, thanks to all the lab mates in Yamada Lab, for many help and advice for my life and research. Special thanks to all members of JUACEP Program, it was great to explore Japan with you and improve my academic research skills simultaneously.

REFERENCES

[1] W. E. Hoogendoorn, et al., “Flexion and rotation of the trunk and lifting at work are risk factors for low back pain: results of a prospective cohort study,” *Spine,* 2000, vol. 25(23), pp. 3087–3092.

[2] G. J. Macfarlane, E. Thomas, A. C. Papageorgiou, P. R. Croft, M. I. Jayson, and A. J. Silman, “mployment and physical work activities as predictors of future low back pain,” *Spine,* 1997, vol. 22(10), pp. 1143–1149.

[3] R. Norman, et al., “A comparison of peak vs cumulative physical work exposure risk factors for the reporting of low back pain in the automotive industry,” *Clinical biomechanics,* 1998, vol. 13(8), pp. 561–573.

[4] A. Burdorf, and G. Sorock, “Positive and negative evidence of risk factors for back disorders,” *Scandinavian journal of work, environment & health,* 1994, pp. 243–256.

[5] B. P. Bernard, and V. Putz-Anderson, “Low-back musculoskeletal disorders: evidence for work-relatedness,” in *Musculoskeletal disorders and workplace factors; a critical review of epidemiologic evidence for work-related musculoskeletal disorders of the neck, upper extremity, and low back,* US Dept. of Health and Human Services, Public Health Service, Centers for Disease Control and Prevention, National Institute for Occupational Safety and Health, 1997, pp. 6-1–6-39.

[6] R. Burgess-Limerick, and B. Abernethy. “Toward a quantitative definition of manual lifting postures,” *Human factors,* 1997, vol. 39(1), pp. 141–148.

[7] S. Mohri, H. Inose, K. Yokoyama, Y. Yamada, I. Kikutani, and T. Nakamura, “Development of endoskeleton type knee auxiliary power assist suit using pneumatic artificial muscles,” in *IEEE International Conference on Advanced Intelligent Mechatronics,* July, 2016, pp. 107–112.

[8] J. R. Potvin, S. M. McGill, and R. W. Norman. “Trunk muscle and lumbar ligament contributions to dynamic lifts with varying degrees of trunk flexion,” *Spine,* 1991, vol. 16(9), pp. 1099–1107.

[9] P. Dolan, A. F. Mannion, and M. A. Adams. “Passive tissues help the back muscles to generate extensor moments during lifting,” *Journal of Biomechanics,* 1994, vol. 27(8), pp. 1077–1085.

[10] Ministry of Health, Labour, and Welfare, “Shokuba ni okeru yotsu yobo taisaku shishin no kaitei no gaiyo toh [Summary of guidelines to prevent occupational diseases]”, 1993.

[11] D. A. Neumann, “Axial skeleton: Muscle and joint interactions,” in *Kinesiology of the Musculoskeletal System-e-book: Foundations for Rehabilitation,* Elsevier Health Sciences, 2013, pp.379–423.

[12] K. B. Hagen, J. Hallen, and K. Harms-Ringdahl, “Physiological and subjective responses to maximal repetitive lifting employing stoop and squat technique,” *European Journal of Applied Physiology and Occupational Physiology,* 1993, vol. 67(4), pp. 291–297.

[13] K. Miura, et al., “The hybrid assisted limb (HAL) for Care Support, a motion assisting robot providing exoskeletal lumbar support, can potentially reduce lumbar load in repetitive snow-shoveling movements,” *Journal of Clinical Neuroscience,* 2018, vol. 49, pp. 83–86.

[14] K. Miura, et al., “The hybrid assistive limb (HAL) for Care Support successfully reduced lumbar load in repetitive lifting movements,” *Journal of Clinical Neuroscience,* 2018, vol. 53, pp. 276–279.

[15] S. Toxiri, et al. “Rationale, implementation and evaluation of assistive strategies for an active back-support exoskeleton,” *Frontiers in Robotics and AI,* 2018, vol. 5, article no. 53.

[16] K. Huysamen, M. de Looze, T. Bosch, J. Ortiz, S. Toxiri, and L. W. O’Sullivan, “Assessment of an active industrial exoskeleton to aid dynamic lifting and lowering manual handling tasks,” *Applied Ergonomics,* 2018, vol. 68, pp. 125–131.

[17] K. S. Stadler, et al., “Robo-mate an exoskeleton for industrial use—concept and mechanical design,” *Advances in Cooperative Robotics,* 2017, pp. 806–813.

[18] T. Bosch, J. van Eck, K. Knitel, and M. de Looze, “The effects of a passive exoskeleton on muscle activity, discomfort and endurance time in forward bending work,” *Applied ergonomics,* 2016, vol. 54, pp. 212–217.

[19] E. P. Lamers, A. J. Yang, and K. E. Zelik, “Feasibility of a biomechanically-assistive garment to reduce low back loading during leaning and lifting,” *IEEE Transactions on Biomedical Engineering,* 2017, vol. 65(8), pp. 1674–1680.

[20] J. Duarte, K. Schmidt, and R. Riener, “The Myosuit: textile-powered mobility,” *IFAC-PapersOnLine*, 2019, vol. 51(34), pp. 242–243.

[21] M. Wehner, et al., “A lightweight soft exosuit for gait assistance,” in *IEEE international conference on robotics and automation,* 2013, pp. 3362–3369.

[22] A. T. Asbeck, R. J. Dyer, A. F. Larusson, and C. J. Walsh, ″Biologically-inspired soft exosuit,” in *IEEE 13th International Conference on Rehabilitation Robotics,* 2013, pp. 1–8

[23] K. Ohashi, Y. Akiyama, S. Okamoto, and Y. Yamada, “Development of a string-driven walking assist device powered by upper body muscles,” in *IEEE International Conference on Systems, Man, and Cybernetics,* 2017, pp. 1411–1416.

[24] S. Naito, Y. Akiyama, K. Ohashi, Y. Yamada, and S. Okamoto, “Development of a non-actuated wearable device to prevent knee buckling,” in *IEEE Global Conference on Life Sciences and Technologies,* 2019, pp. 247–249.

[25] F. Sibella, M. Galli, M. Romei, A. Montesano, and M. Crivellini, ″Biomechanical analysis of sit-to-stand movement in normal and obese subjects,” *Clinical biomechanics,* 2013, vol. 18(8), 745–750.

[26] A. Fattah, M. Hajiaghamemar, and A. Mokhtarian, “Design of a Semi-Active Semi-Passive Assistive Device for Sit-to-Stand Tasks,” presented at the 16th Annual (International) Conference on Mechanical Engineering-ISME2008, Shahid Bahonar University of Kerman.

Effect of Different Orientations of Compensation Chamber on Loop Heat Pipe System for Automobiles

Guanru Feng
Department of Mechanical Engineering, University of Michigan
gfeng@umich.edu

Yoshitada Aono
Thermal Control Engineering Group, Nagoya University
aono.yoshitada@i.mbox.nagoya-u.ac.jp

Supervisor: Prof. Hosei Nagano
Thermal Control Engineering Group, Nagoya University
nagano@mech.nagoya-u.ac.jp
(Dated: August 27, 2019)

The purpose of this project is to compare the loop heat pipe efficiency under different working conditions. The variables include different orientations of the compensation chamber and different convection cooling method of condenser. Combinations between vertical and horizontal compensation chamber placement and natural-air, forced-air and natural-water convection cooling are investigated. The vertical compensation chamber with natural-water convection shows the best performance.

I. INTRODUCTION

In the recent years, energy conservation and global warming are attracting more attentions. Thus, automobiles, the daily transportation which consumes fossil fuels and discharge waste gases, draw more researchers eyes. Alternative energy sources such as hydrogen, electricity and hybrid energy are being researched and applied on automobiles. However, before these alternative energy resources become feasible and convenient for people to use in daily life, the main efforts should still be concentrated on the improvement of the thermal efficiency of automobiles. The thermal efficiency of internal combustion engine powered by gasoline and diesel is around 30% and the rest thermal energy is excreted as waste heat. Therefore, if we were able to recycle the waste heat and make use of it, the efficiency of the fuels can be increased.

Loop heat pipe (LHP)[1] is one of the solutions to resolve this problem. LHP is a two-phase-working engineering system, which is composed mainly of an evaporator, a compensation chamber and a condenser so that it can transfer heat in an efficient way. The waste heat from the engine can be used as a heat source of the evaporator. With the help of working fluids such as water or ammonia, heat can be transferred a long distance through pipes to the condenser. The compensation chamber will store the excess working fluid. Thus, not only does LHP has a relatively higher heat conductivity than solid materials, but it also has the advantage of self-starting and good long-distance heat transfer capacity. In this research, we will investigate the effects of different orientations of evaporator and compensation chamber on the loop heat pipe systems.

II. DESIGN MODEL

A. LHP Setup

The whole loop heat pipe system, as shown in the schematic diagram in Figure 1, is composed of a compensation chamber, an evaporator, a wick and a condenser, which are all connected by pipes. All components are manufactured with stainless steel. Figure 2a shows the flow direction of the working fluids.

Heat sources are attached on both the top and bottom surface of the evaporator, where the working fluid is vaporized. Figure 2b shows the cross-section (A-A). The wick with three cores is inserted into the evaporator with no space in between. Working fluid flows in the cores through the bayonet tubes and then is vaporized. Vapor flows through the pores on the wick and the groove into the vapor line, which is connected to the condenser. In the condenser, heat transfer occurs. As the heat energy dissipates from the condenser to the ambient, the vapor is condensed to liquid and enter the liquid line, through which the liquid working fluid flows into the compensation chamber (CC). CC is used to store the excess working fluid before they are vaporized in the evaporator. The whole LHP system except the condenser is covered by the insulation materials. The condenser is 25cm higher than the evaporator such that vapor working fluid will flow smoothly in the vapor line due to low density and liquid working fluid will flow smoothly in the liquid line due to gravity.

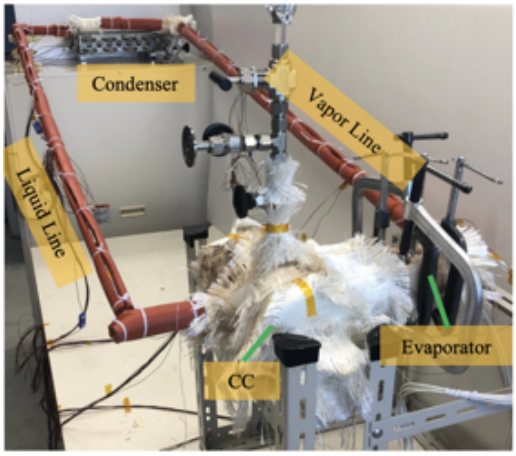

FIG. 1: Loop heat pipe set up

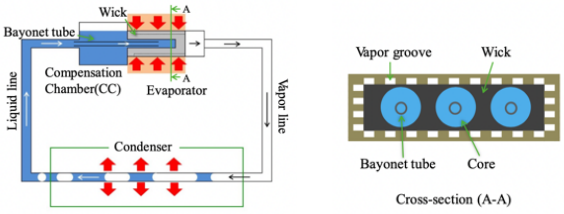

(a) (b)

FIG. 2: (a) Flow direction, (b) cross-section at (A-A) surface

B. Thermodynamic Analysis

The pressure-temperature diagram in Figure 3 represents the steady-state operation of LHP system. At state 1, the vapor is at saturated temperature corresponding to the highest pressure in the system. As vapor working fluid travels through the grooves to state 2, temperature is increased due to the heat convection from the heat sources, and pressure drops. In the vapor line, temperature is kept the same by the insulation materials covered on the pipes. Pressure decreases to state 3 because of the friction losses. From state 3 to state 6, working fluid is in the condenser. During condensation process, state 4 to state 5 represents the liquid-vapor interface. Depending on how much thermal energy is supplied to the evaporator, the liquid-vapor interface position can vary between the inlet and the outlet of the condenser. Therefore, state 4 and state 5 can move along the saturation line. After condensation, the liquid phase working fluid travels through the insulated liquid line from state 6 to state 7 with pressure drop due to frictional loss but no temperature change due to insulation. As the liquid phase working fluid reaches the CC inlet at state 7, it is heated by the heat leak from the evaporator to state 8, which is the outlet of the CC. The process from state 8 to state 9 represents the liquid flow through the wick into

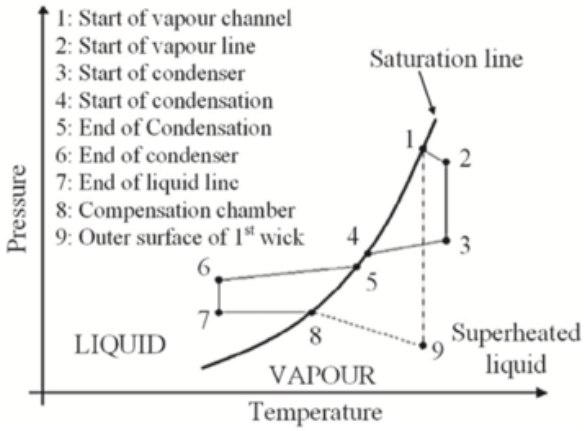

FIG. 3: Ideal P-T diagram showing the working principle of LHP system
[2]

the evaporation zone. During this period, working fluid is super-heated, but doesn't boil in a very short period of time. Pressure loss happens as the working fluid flows through pores of the wick.

Aforementioned is the ideal thermodynamic analysis. In real-world application, working fluid may move directly from state 8 to state 1 along the saturation line, as the capillary action and the evaporation may happen simultaneously.

Loop heat pipe is a passive engineering system mainly driven by the pressure drop within each component. Thus, the pressure increase should be greater than the pressure drop so that the loop heat pipe will work properly. The governing pressure equation is

$$P_{cap}+\Delta P_g \geq \Delta P_{vl}+\Delta P_{ll}+\Delta P_{con}+\Delta P_{wick}+\Delta P_{gr} \quad (1)$$

where cap, g, vl, ll, con and gr stand for capillary, gravity, vapor line, liquid line, condenser and groove, respectively. Capillary pressure can be calculated by

$$P_{cap} = \frac{2\sigma\cos(\theta)}{r_{pore}} \quad (2)$$

where σ is surface tension, θ is contact angle between fluid and pore inner surface and r_{pore} is pore radius.

C. Components and Dominant Formulae

Loop heat pipe system is a self-started thermal energy transfer design. Capillary force generated in the wick will drive working fluid from the compensation chamber into the evaporator. The flow in the LHP system is motivated by the pressure drop between each component. Table I shows the geometric measurements of each component.

TABLE I: Geometry measurements of all components in millimeter

	Length	Width	Height
Heat Block	100	100	16
Evaporator	153	112	40
Wick	130	100	30
Groove	110	2.5	2.5
	Length	Inner Diameter	Outer Diameter
Condenser	5000	12.7	10.7
Vapor Line	2100	19.05	16.57
Liquid Line	2000	9.525	7.745

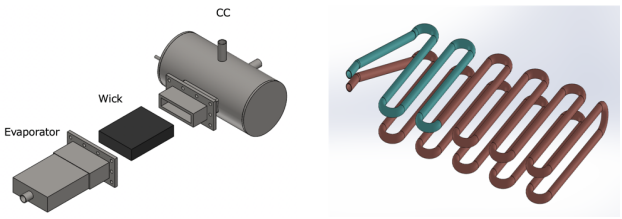

(a) (b)

FIG. 4: (a) CAD model of CC, Wick and evaporator, (b) CAD model of condenser

1. Compensation Chamber

Compensation chamber, as shown in Figure 4a, has a volume of 3.07L. It is used to store the excess working fluid and supply the wick with liquid working fluid at all times. No pressure drop happens in the compensation chamber. Working fluid exists as both liquid and vapor states. The vapor phase and liquid phase volumes in the compensation chamber are

$$V_v = (\rho_l V_{cc} - M_{cc})/(\rho_l - \rho_v) \tag{3}$$

$$V_l = (M_{cc} - \rho_v V_{cc})/(\rho_l - \rho_v) \tag{4}$$

where M is the working fluid mass in the compensation chamber.

The working fluid in the compensation chamber receives the heating of the radial heat leak from the evaporator, the cooling of the return cooled liquid and a heat transfer with the CC casing.

2. Vapor, Liquid Lines

Liquid line and vapor line are all simple pipes covered by insulation materials. These two pipes only have working fluid in single phase. Frictional pressure loss occurs as the single phase working fluid flows through pipes. The pressure drop can be calculated by

$$-\frac{dP}{dL} = f \times \frac{\rho u^2}{2} \times \frac{4}{d_i} \tag{5}$$

where L, ρ, u and d_i stand for pipe length, fluid density, fluid flow velocity and inner diameter of pipe, respectively. The frictional factor is calculated from Reynolds Number as follows:

$$f = \begin{cases} 16/Re & \text{when } Re < 2200 \\ 0.0791 \times Re^{-0.25} & \text{when } 2200 < Re < 10^5 \end{cases} \tag{6}$$

The energy conservation equation of the working fluid in the transport lines is as follow

$$-\dot{m} C_p \frac{dT}{dL} = G_{i\_amb}(T_i - T_{amb}) \tag{7}$$

where C_p is the specific heat of the working fluid and G_{i_amb} is the heat transfer coefficient between the working fluid and the ambient.

3. Evaporator

Evaporator, as shown in Figure 4a, is used to vaporize the working fluid. Working fluid flows in the evaporator and the wick, where it will be vaporized. The evaporator receives thermal energy directly from the heat block and this heat transfer can be calculated by

$$Q_{load} = G_{HB,e} \times (T_{HB} - Te) \tag{8}$$

where Q_{load} is generated by heat source and $G_{HB,e}$ is the thermal conductance coefficient between heat block and evaporator. One part of this heat is transferred to compensation chamber as radial heat leak and the other part will be used to vaporize the working fluid.

There are 40 grooves that are manufactured inside the evaporator. The pressure drop through the grooves can be calculated by Eq. (5).

4. Wick

Wick, as shown in Figure 4a, composes of three cores with a porosity of 0.4 and pore size of 1.2μm in radius. Working fluid is supplied through three bayonet tubes into the wick. As thermal energy is transferred from heat sources, working fluid flows through the pores on the wick into the vapor line and evaporation occurs. Meanwhile, pressure change can be calculated by Darcy's Law[3] as

$$\Delta P_{wick} = \frac{\dot{m}\mu \ln(r_o/r_i)}{2\pi\rho K_{wick} L_{wick}} \tag{9}$$

where $\dot{m}$ is mass flow rate, μ is viscosity of fluid, r_o is outer radius, r_i is inner radius, K is permeability of formation and L is wick length.

Wick receives thermal energy from the evaporator and can be calculated as

$$Q = \frac{k_{eff} L_{wick} w_{wick}}{h_{wick}} \times \Delta T \tag{10}$$

where h is the heat transfer coefficient. The effective thermal conductivity is calculated as

$$k_{eff} = {k_{max}}^{0.42} \times {k_{min}}^{0.58} \tag{11}$$

$$\begin{cases} k_{max} = \epsilon k_l + (1-\epsilon) k_{wick} \\ k_{min} = \frac{k_l k_{wick}}{\epsilon k_{wick} + (1-\epsilon) k_l} \end{cases} \tag{12}$$

where ϵ is the porosity of the wick.

5. Condenser

Condenser, as shown in Figure 4b, dissipate thermal energy to the ambient, and working fluid is condensed. Therefore, liquid and vapor states co-exist in the condenser. The pressure drop in the single-phase region can be calculated by Eq. (5). The two-phase region pressure drop can be calculated as

$${\Phi_j}^2 = \frac{\Delta P_{2p}}{\Delta P_j} \tag{13}$$

where Φ and X are Lockhart-Martinelli parameters [4] and can be calculated as

$$\begin{cases} {\Phi_l}^2 = 1 + cX + X^2 \\ {\Phi_v}^2 = 1 + \frac{c}{X} + \frac{1}{X^2} \end{cases} \tag{14}$$

$$c = \begin{cases} 5 & \text{if } Re_v < 2300, Re_l < 2300 \\ 10 & \text{if } Re_v < 2300, Re_l \geq 2300 \\ 12 & \text{if } Re_v \geq 2300, Re_l < 2300 \\ 20 & \text{if } Re_v \geq 2300, Re_l \geq 2300 \end{cases} \tag{15}$$

$$X = \frac{\Delta P_l}{\Delta P_v} \tag{16}$$

The dominant energy equation is related to the vapor quality ranging from 1 to 0 from the inlet to the outlet of the condenser.

$$\frac{dx}{dz} = \frac{1}{\dot{m}\lambda} G \Delta T \tag{17}$$

where x stands for the vapor quality, z stands for the length of condenser pipe, λ represents the latent heat of vaporization.

6. Thermocouple

Thermocouple are attached on the whole LHP system to measure the local temperature. As shown in the Figure 5a, red dots are the positions of thermocouple. Figure 5b shows the thermocouple positions on the evaporator and CC. After the local temperature measurements are collected, the average temperature will be calculated.

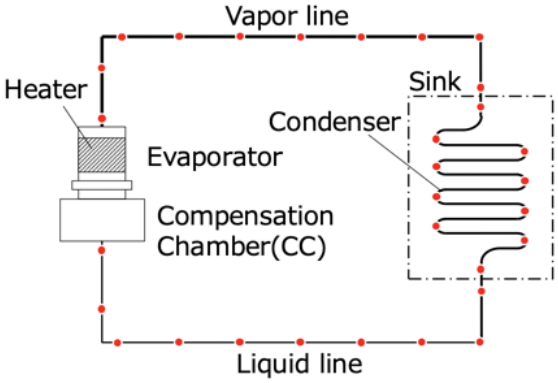

(a)

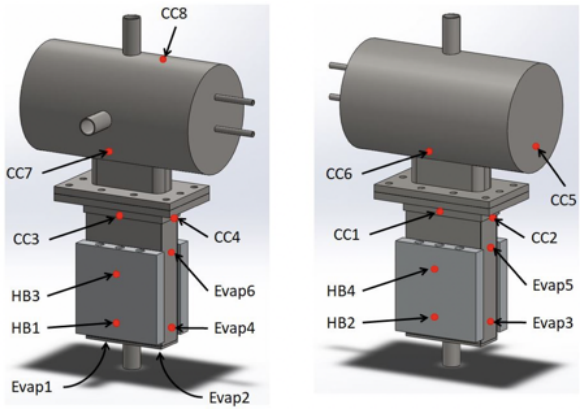

(b)

FIG. 5: (a) Thermocouple position on the LHP system, (b) Thermocouple position on the evaporator and CC

7. Working Fluid Volume

Because compensation chamber serves as the working fluid supply to the wick, there is a minimum volume requirement in the CC such that enough working fluid will be supplied during operation. During the working fluid pouring process, all components will be fully filled before the compensation chamber. Thus, the minimum working fluid volume for the loop heat pipe to work is the sum of the minimum volume requirement of the compensation chamber and the volume of all the other components.

Because the vapor phase has a smaller density than liquid phase, the maximum liquid working fluid volume occurs when the vapor working fluid is at the maximum volume. Vapor phase can only exist in the groove, vapor line and condenser. When the condensation is finished at the outlet of the condenser, vapor phase reaches its maximum volume. Under this circumstance, the maximum working fluid volume for the loop heat pipe to work is the sum of the volume of compensation chamber, wick and liquid line.

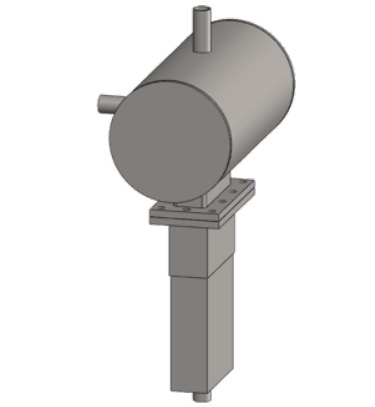

(a)

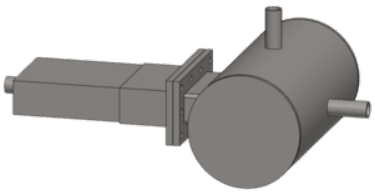

(b)

FIG. 6: (a) Vertical orientation compensation chamber, (b) Horizontal orientation compensation chamber

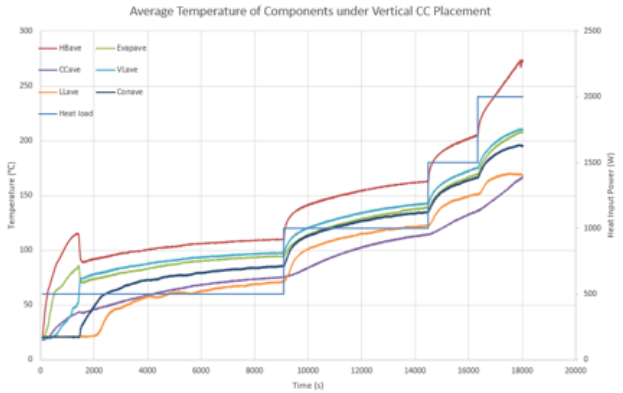

(a)

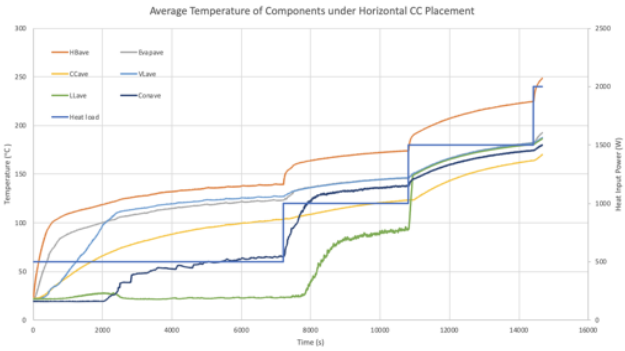

(b)

FIG. 7: (a) Natural-air convection method with vertical CC placement, (b) Natural-air convection method with Horizontal CC placement

III. RESULTS AND DISCUSSIONS

This research is based on variable control method. The two variables that will be investigated through experiments are the compensation chamber orientations and condenser cooling methods. The compensation chamber orientations include the vertical and horizontal placements as shown in Figure 6. The cooling methods of the condensers are natural-air convection, forced-air convection and natural-water convection. Because the main working principle of the condenser is to make heat exchange with the ambient. Therefore, the ambient temperature is fixed at 24°C. The working fluid is decided to be water, the most feasible and easiest-to-get fluid with a high latent heat of vaporization. The volume of total water inside loop heat pipe is 2750cc. The experiment will stop when heat block temperature reaches 300°C or compensation chamber temperature reaches 200°C.

A. Natural-Air Convection Method

The natural-air convection cooling method is shown in Figure 1. The condenser contacts the ambient environment directly with only the heat transfer due to the temperature difference between the condenser and the ambient. Under this cooling method, Figure 7 shows the average temperature of each component as time passes by and heat load increases. The blue lines shows the step-increased heat load input. As shown in Section II B and Figure 3, the condenser is used to make heat transfer with the ambient environment and the working fluid will condense from vapor to liquid. During the condensation, the temperature of the working fluid will remain the same. It is clear that the average condenser temperature curve is between the average vapor line temperature and the average liquid line temperature curves. This indicates that the working fluid is fully condensed in the condenser.

When heat load is below 1000W, the average temperatures of the evaporator, compensation chamber and vapor line are lower under the vertical placement rather than the horizontal placement, while the liquid line and condenser have lower temperatures. When the heat load continues to increase, all components under the horizontal compensation chamber placement condition will have higher average temperatures.

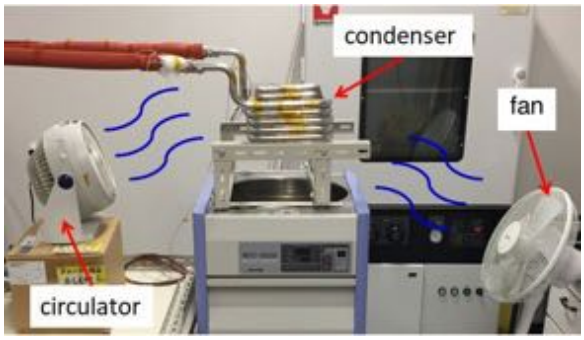

(a)

(b)

FIG. 8: (a) Experiment Setup under forced-air convection cooling method, (b) Experiment Setup under natural-water convection cooling method

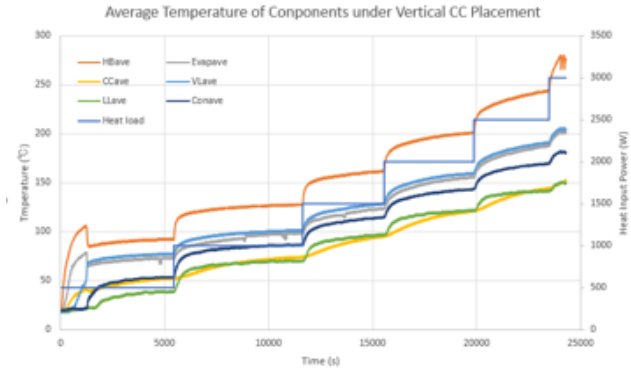

(a)

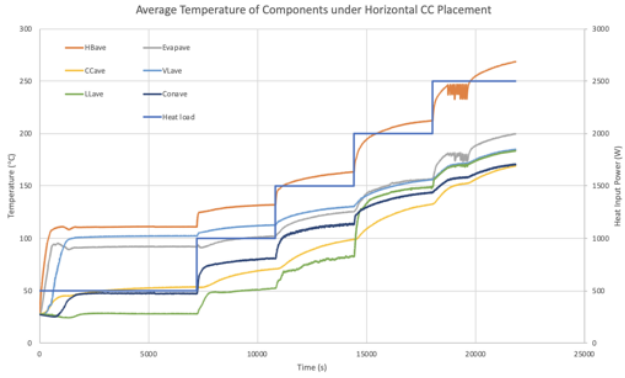

(b)

FIG. 9: (a) Forced-air convection method with vertical CC placement, (b) Forced-air convection method with Horizontal CC placement

B. Forced-Air Convection Method

The forced-air convection cooling method is shown in Figure 8a. The condenser contacts the ambient environment directly with one fan and one circulator generating air flows to speed up heat transfer rate. Under this cooling method, Figure 9 shows the average temperature of each component as time passes by and heat load increases. Aforementioned, the gap between the average vapor line and liquid line temperatures shows the completion of the condensation process inside the condenser.

In Figure 9b, the fluctuation of the average evaporator temperature when the heat load is 2500W is caused by the fluctuation of the average heat block temperature. The possible source of this error may comes from the loose contact between the heat block and the heat block power supply. The sudden drop of the average temperatures of the evaporator and the heat block in Figure 9a may comes from the same source of error.

Compared the vertical and horizontal compensation chamber placement, as shown in Figure 9, the average temperatures of components don't have a clear difference between two placement conditions.

C. Natural-Water Convection Method

The natural-water convection cooling method is shown in Figure 8b. The condenser is put in the tank filled with water initially at ambient temperature and is fully immersed in the tank water. Under this cooling method, Figure 10 shows the average temperature of each component as time passes by and heat load increases.

In Figure 10b, there are three clear fluctuations in the average temperature of the tank water. Initially, the tank is fully filled with water at 1 atmosphere pressure and ambient temperature of 24°C. As the heat load is increasing, the condenser temperature increases, resulting in the increase in the difference of the condenser temperature and the tank water temperature. More heat transfer occurs and the temperature of the tank water rises. When the water reaches 100°C, the boiling point under 1 atmosphere pressure, it starts to vaporize. Thus, the volume of the tank water decreases. To keep the condenser fully immersed in the tank water, more water at the ambient temperature is added into the tank. Therefore, the average temperature of the tank water is driven down suddenly.

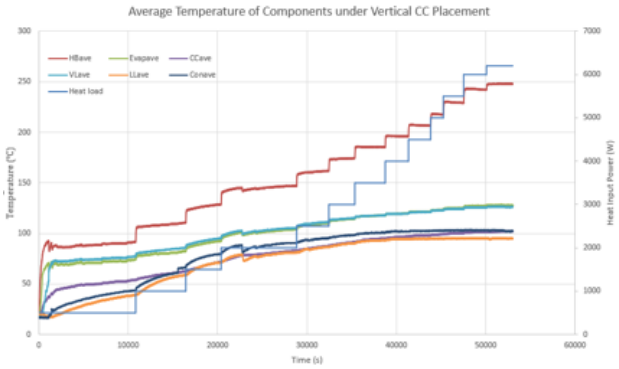

(a)

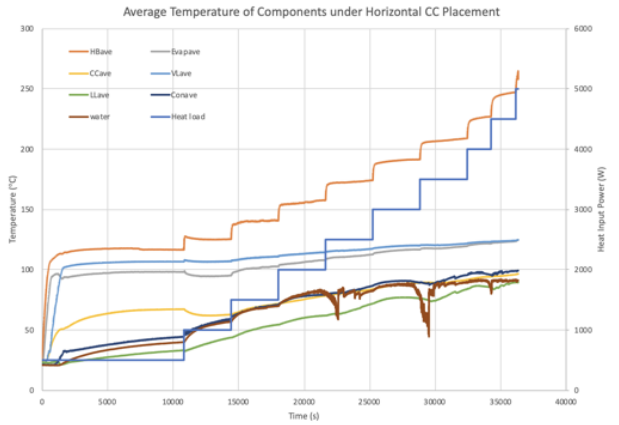

(b)

FIG. 10: (a) Natural-water convection method with vertical CC placement, (b) Natural-water convection method with Horizontal CC placement

As shown in Figure 10, the rates of the increase in the average temperature of all components are slowing down, because condenser can release more thermal energy when it is making heat exchanging with tank water due to the high heat capacity of liquid water. Even when heat load increases up to 5000W, the LHP will work properly.

D. Thermal Resistance Comparison

Compared all the experiment results under the horizontal compensation chamber placement condition, as shown in Figure 7b, 9b and 10b, the natural-water cooling method results in the lowest average temperatures of the liquid line and the condenser as expected. This is because water has a high heat capacity and latent heat of vaporization. The forced-air convection method shows lower temperatures of the liquid line and the condenser than the natural-air convection method, due to the heat transfer caused by the air flow generated by fans.

However, the temperatures of the liquid line and the condenser solely cannot determine the performance of the

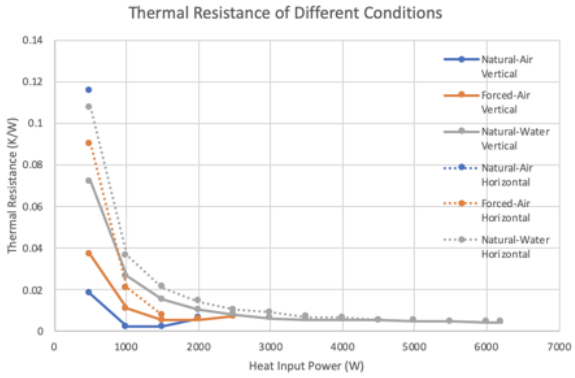

FIG. 11: Thermal Resistance of different compensation chamber orientations and cooling methods

loop heat pipe system under different conditions. A new parameter, thermal resistance, is introduced. Thermal resistance to the temperature difference is what electrical resistance to the potential difference. Thus, the equation to calculate thermal resistance is

$$R_t = \frac{\Delta T}{q} \tag{18}$$

where R_t represents thermal resistance and q represents rate of heat flow.

If loop heat pipe system is considered as one integrated system, the only inlet for heat flow is the heat block and the only outlet for heat flow is the condenser. Thus, in Eq. (18), the temperature difference between the evaporator and the condenser is the ΔT and the heat power supply is the q. The calculated thermal resistance for each placement condition and cooling method is shown in Figure 11. It is clear that vertical compensation chamber orientation has a lower thermal resistance rather than the horizontal orientation and thus a better performance in transferring heat. In the vertical loop heat pipe, gravity will work as an additional driven force to supply the wick with liquid water from the compensation chamber. Among three vertical compensation chamber orientation conditions, when heat load is lower than 2500W, the natural-air convection has the lowest thermal resistance. While the heat load is increased above 3000W, natural-water convection method will be the best choice.

IV. CONCLUSION AND FUTURE WORKS

At a low heat power supply below 2000W, natural-air convection method with vertical compensation chamber is the most proper selection to make long-distance heat transfer. However, at a high heat power supply above 3000W, natural-water convection method with vertical compensation chamber orientation will generate the best performance with the lowest thermal resistance. Future

work will focus on the forced-water convection method, in which the tank water will be flowing rather than stationary. An additional research direction is to investigate the effect of the tilted compensation chamber orientations.

ACKNOWLEDGMENTS

I wish to acknowledge the support of the Japan-US-Canada Advanced Collaborative Education Program for the visiting graduate student opportunity. I wish to thank Professor Hosei Nagano and lab members of Thermal Control Engineering Group for the suggestions and advice during the research.

[1] Y. Maydanik, Loop heat pipes (2005).
[2] A review of small heat pipes for electronics, Applied Thermal Engineering **96**, 1 (2016).
[3] L. Bai, G. Lin, H. Zhang, and D. Wen, Mathematical modeling of steady-state operation of a loop heat pipe, Applied Thermal Engineering **29**, 2643 (2009).
[4] R. W. Lockhart, Proposed correlation of data for isothermal two-phase, two-component flow in pipes (1949).
[5] M. Mitomi and H. Nagano, Long-distance loop heat pipe for effective utilization of energy, International Journal of Heat and Mass Transfer **77**, 777 (2014).

Inserted Wedge-shaped CoFe Layer Studied by Time-Resolved Magneto-optical Kerr Effect (TR-MOKE)

Yu-Ching Hsiao
Mechanical and Aerospace Engineering, UCLA

Advisors
Prof. Satoshi Iwata, Prof. Takeshi Kato, Prof. Daiki Oshima
Institute of Materials and Systems for Sustainability, Nagoya University

Abstract

The interface of CoFeB and MgO exhibits perpendicular magnetic anisotropy (PMA), which has been widely used for high density non-volatile memories[1][2]. Here, we proposed the structure Si/Ta(2 nm)/ CoFeB(0.9 nm)/CoFe(0.14-0.45 nm)/MgO(3 nm)/Ta(2 nm). A wedge-shaped CoFe layer was inserted to engineer magnetic anisotropy and observe spin-reorientation transition (SRT) across in-plane to out-of-plane. Magneto optical spectrometer was utilized to discover the samples of SRT region[3]. We investigate the samples with Time-Resolved Magneto-optical Kerr Effect (TRMOKE). Materials properties: damping coefficient, g-factor and effective anisotropy field were obtained from the measured data fitted with oscillation function. We found damping coefficient decreases from 0.00947 to 0.00755 as thickness of CoFe increases from 0.31 to 0.35 (nm). The results would help to design the low power magnetization switching memory device.

Introduction

Perpendicular magnetic anisotropy (PMA) has been widely used for high-density magnetoresistive random-access memory (MRAM) [4]. CoFeB/MgO is one of most studied structures to achieve low damping coefficient, which is essential for STT-MRAM to reduce the critical current for switching magnetization[cite]. In this work, a wedge-shaped CoFe was inserted between CoFe and MgO layer to engineer the anisotropy. We investigate thickness dependency of damping coefficient and other magnetic dynamic properties.

In this work, time-Resolved Magneto-optical Kerr Effect (TR-MOKE) was utilized to study magnetic dynamics of the proposed wedge-shaped CoFe structure[5], [6]. Ultra-short pulse laser (~100 fs) of TR-MOKE system enables us to study fast switching magnetization, especially useful for strong anisotropy materials. The ferromagnetic resonance frequency of our propsoed structure reaches GHz with large external applied field (~Tesla). Thus, TR-MOKE becomes essential.

Background

Time-Resolved Magneto-optical Kerr Effect (TRMOKE)

TR-MOKE is a pump probe system to study ultra-fast dynamics magnetization. TR-MOKE setup was shown in Fig. 1. The emitted laser was first split into two beams by half-wave plate

polarized beam splitter. The strong probe laser was tuned to 520 nm after passing second harmonic generator whereas the weak pump laser wavelength remains 1040 nm.

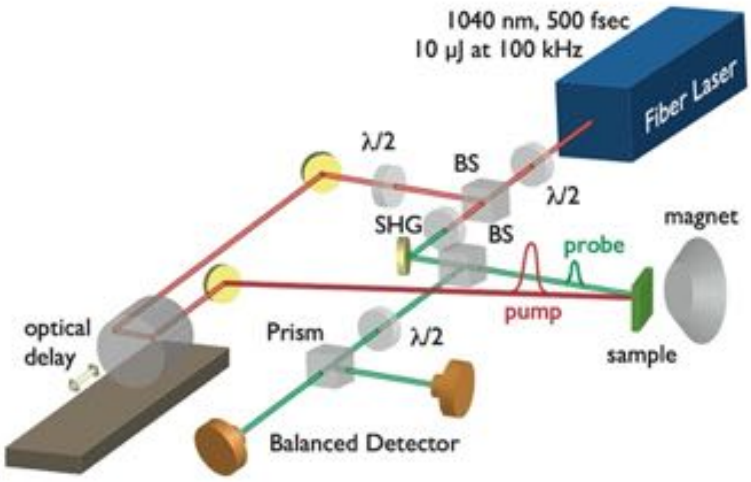

Figure 1. Set-up of TR-MOKE system

Pump laser with delay time was incident on the sample. Fig. 2 demonstrates the magnetization change in the pump process. The sample was applied with the external field at a selected angle. Effective field is the sum of applied magnetic field and effective anisotropy field as shown in Fig. 2(a). Pump laser induces thermal demagnetization and weakens anisotropy effective field of the sample. The demagnetized spin state was recovered back to the original state within pico seconds (See in Fig. 2(b)). The precession motion is monitored by the probe laser which is reflected back to the detector and measure the change of Kerr signal. The measured data can be fitted with the oscillation function:

$$A \exp\left(-\frac{t}{\tau}\right) sin\omega t \tag{1}$$

where τ is the relaxation time, ω indicated the angular frequency of oscillation and t is the delay time.

(a) (b)

Figure 2. The magnetization state (a) beofore pump, at delay time = 0 (b) afeter pump, at delay time > 0

Wedge-shaped Structure

Fig. 3 indicates the cross section of the proposed wedge-shaped structure. The multilayers were prepared on the polycrystalline Si substrate by magneton sputtering at the room temperature. Ta was chosen as the seed layer and followed with CoFeB/MgO structure and capped with Ta. The gradual thickness of CoFe was obtained by the different angles from the source target shown in Fig. 4. The thickness of wedge-shaped CoFe was determined using Eq. (2):

$$thickness = \frac{t_c}{1.5}(0.026x + 1.47)(nm) \quad (2)$$

where t_c represents center thickness and x indicated the distance in mm from the center of sample.

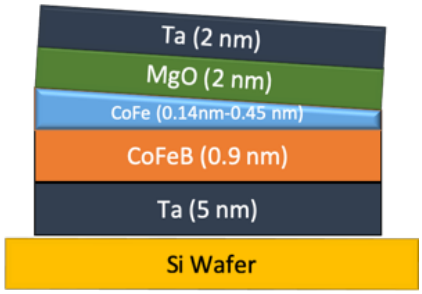

Figure 3. The cross section of the structure

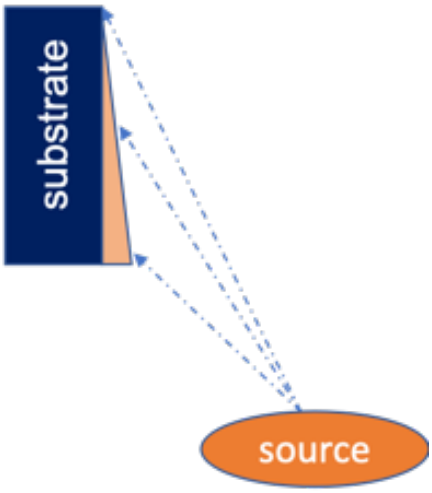

Figure 4. The approach to achieve gradual change of thickness with sputtering

Results and Discussion

Magneto-optical Kerr effect characterization

The spin reorientation transition (SRT) region are studied for its dynamical properties using TR-MOKE. SRT indicates the transition region from in-plane magnetization to out-of-plane

magnetization. The transition is achieved by the inserted layer of varying CoFe thickness. To test thickness dependency, the wedge-shaped sample was cleaved into pieces. The thickness of each piece was calculated by Eq. (2). Fig. 5 shows the corresponding thickness with respect to the position of the sample. In order to find the spin transfer transition region, the sample was characterized with magneto optical spectrometer in Iwata Lab. The positions at the labeled number 1-3 were observed with the in-plane to out-of-plane transition. Fig. 6 demonstrated the hysteresis loops of SRT. At the 500 Oe external field, magnetization switches 180 degrees in Fig. 6(c), as opposed to Fig. 6(a) exhibiting in-plane easy axis. Fig. 6(b) indicates the transition state between in-plane and out-of-plane states.

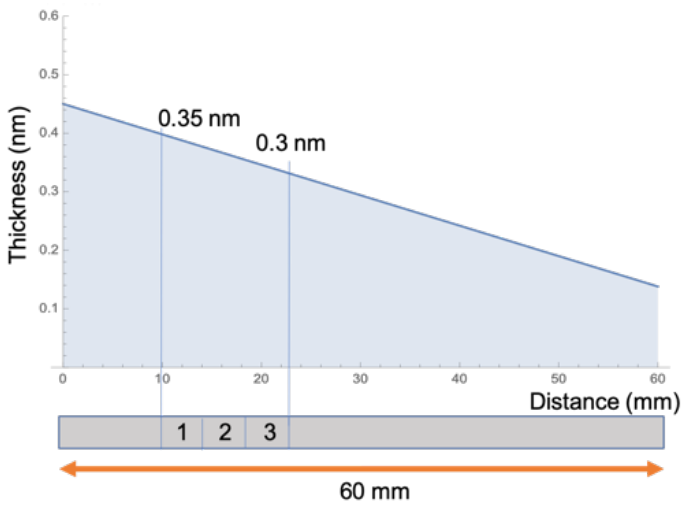

Figure 5. CoFe thickness change with respect to the position of the wedge-shaped sample

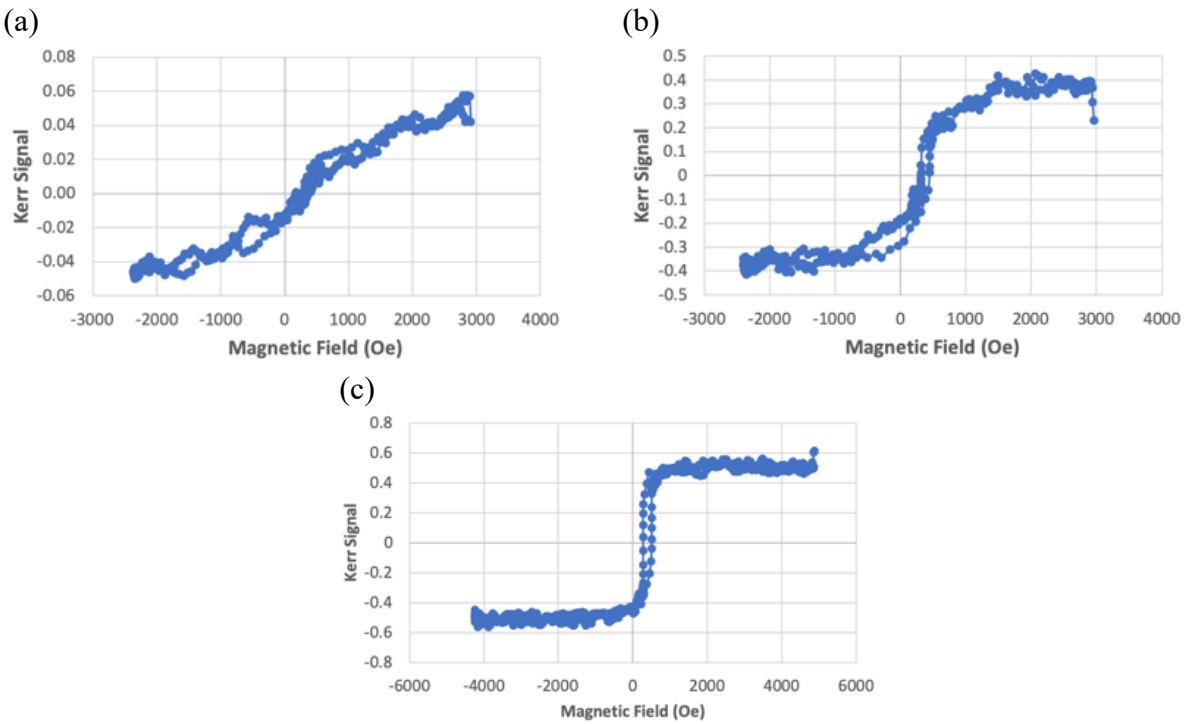

Figure 6. Hysteresis loop characterized by Magneto spectra measurement for (a) sample 1 with nominal CoFe thickness of 0.35 nm (b) sample 2 with nominal CoFe thickness of 0.33 nm (c) sample 3 with nominal CoFe thickness of 0.31 nm

TR-MOKE characterization

Samples 1-3 were selected to investigate dynamic magnetization properties with TR-MOKE. Laser of wavelength 1040 nm, pulse width 500 fs and repetition frequency was set for TR-MOKE. The external field 0.8 T to 1.4 T with increments of 0.1 T was applied to the sample at the angle of 60 degrees from the film normal direction. In the case of sample 1, pump laser 60 mw and probe laser 180 μw were used. The extracted and fitted data with varying applied magnetic fields was shown in Fig. 7.

Damping coefficient (α) is one of important materials properties that can be obtained by TR-MOKE. With varied external fields, the fitted curves spinwave dispersion (ω) and the inverse lifetime of spinwave ($\delta\omega$) versus external magnetic field of sample 1 were shown in Fig. 8. Damping coefficient can then be obtained using Eq. (3):

$$\alpha = \frac{\delta\omega}{2\omega} \tag{3}$$

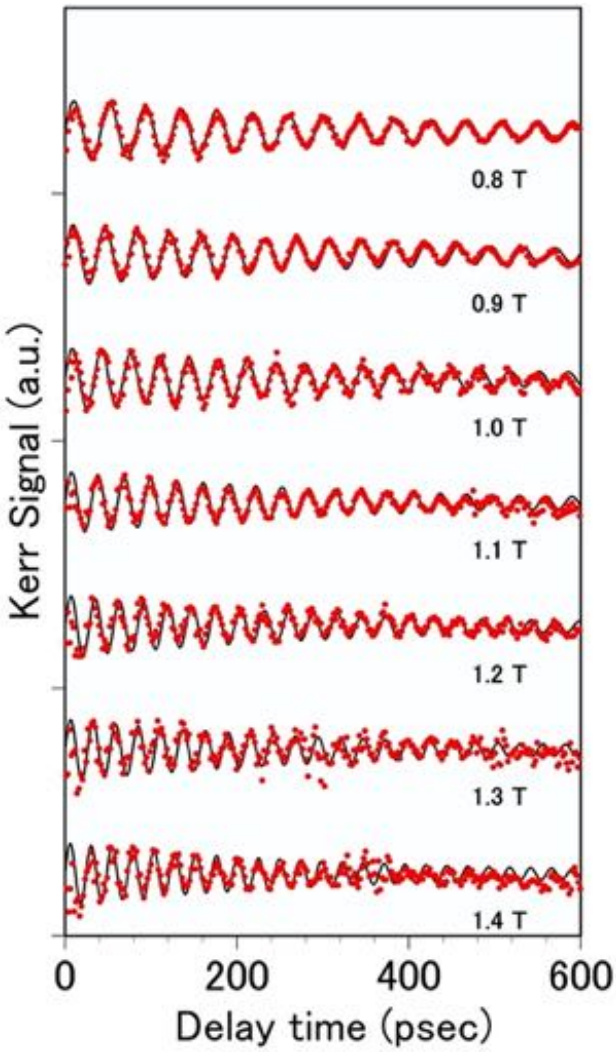

Figure 7. TR-MOKE waveforms with varying external magnetic applied field from 0.8-1.4 T. The red dots represent measured data points and black curves indicate fitted oscillation function.

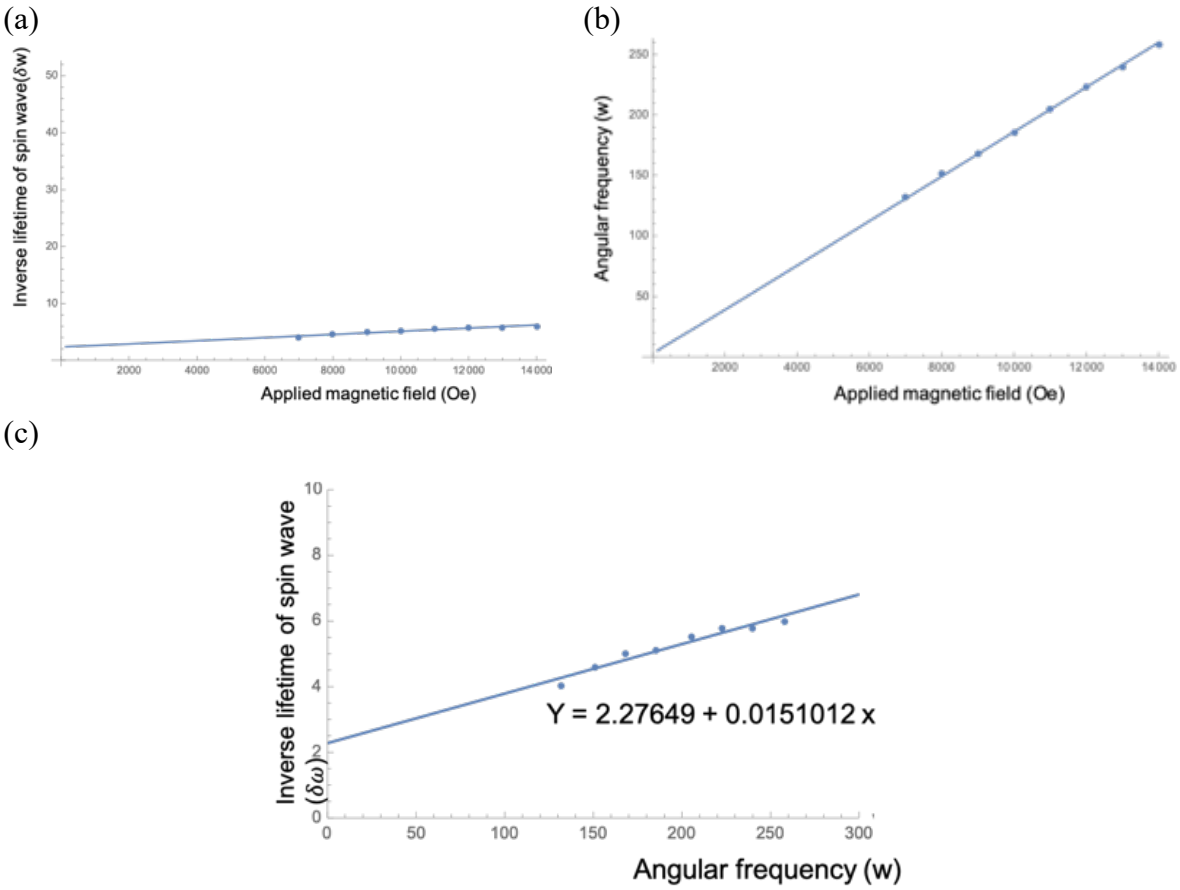

Figure 8. The fitted curves of (a) spinwave dispersion (ω) versus external magnetic field (b) the inverse lifetime of spinwave ($\delta\omega$) versus external magnetic field (c) damping coefficient obtained from the slope

Materials properties: damping coefficients, g-factor and effective anisotropy field were acquired for sample 1-3 and presented in Table. 1. As the thickness of CoFe decreases, the damping coefficient increases. CoFe of low thickness has less amount of total magnetic moment. Therefore it requires lower energy barrier for magnetization switching with same spin current flow. This results in higher energy loss and thus large damping coefficient.

Sample	Thickness	Easy axis	Damping coefficient	g-factor	H_{keff} (Oe)
#1	0.35	IP	0.00755	2.05	-1800
#2	0.33	IP-OOP	0.00827	2.05	-500
#3	0.31	OOP	0.00947	2.05	500

Table 1. TR-MOKE characterization results of sample 1-3

Conclusion

In this study, wedge-shaped CoFe structure was fabricated and characterized by magneto optical spectroscopy and TR-MOKE to investigate magnetic dynamics. In plane to out of plane magnetization was observed at the position of sample 1-3. The selected samples were measured by TR-MOKE. Damping coefficient, g-factor and effective anisotropy field were obtained from the measured data and fitted curves. The results show that the damping coefficient increases as the thickness of CoFe decreases. Understanding the thickness dependency of damping coefficient enables us to design energy efficient memory device.

References

[1] "Dependence of magnetic properties of MgO/CoFeB/Ta stacks on CoFeB and Ta thicknesses," 2015.

[2] S. Ikeda *et al.*, "A perpendicular-anisotropy CoFeB–MgO magnetic tunnel junction," *Nat. Mater.*, vol. 9, no. 9, pp. 721–724, Sep. 2010.

[3] J.-W. Lee, J.-R. Jeong, S.-C. Shin, J. Kim, and S.-K. Kim, "Spin-reorientation transitions in ultrathin Co films on Pt(111) and Pd(111) single-crystal substrates," *Phys. Rev. B*, vol. 66, no. 17, p. 172409, Nov. 2002.

[4] Y. Huai, "Spin-Transfer Torque MRAM (STT-MRAM): Challenges and Prospects," 2008.

[5] T. Kato, D. Oshima, and S. Iwata, "Ion irradiation for planar patterning of magnetic materials," *Crystals*, vol. 9, no. 1. MDPI AG, 01-Jan-2019.

[6] T. Kato, K. Nakazawa, R. Komiya, N. Nishizawa, S. Tsunashima, and S. Iwata, "Compositional dependence of g-factor and damping constant of GdFeCo amorphous alloy films," in *IEEE Transactions on Magnetics*, 2008, vol. 44, no. 11 PART 2, pp. 3380–3383.

The 25th JUACEP Workshop

for the summer research course students from University of Michigan and UCLA

Date: Friday, August 30, 2019

Venue: IDEA STOA (Ground floor, NIC)

Timetable

(15 min. talk + 4 min. Q&A each)

10:10 – 10:20 Opening address
by Prof. Mizutani, Dean of Graduate School of Engineering

10:20 - 10:40 **Yu-Ching Hsiao** …*Advisor: Prof. Satoshi Iwata, Electrical Engineering*
"Inserted Wedge-shaped CoFe Layer Studied by Time-Resolved Magneto-optical Kerr Effect (TRMOKE)" p.37

10:40 – 11:00 **Guanru Feng** …*Advisor: Prof. Hosei Nagano, Mechanical Systems Engineering*
"Effects of Different Orientations of Compensation Chamber on Loop Heat Pipe System on Automobiles" p.40

11:00 – 11:20 **Chen-Yu Cheng** …*Advisor: Assoc. Prof. Shogo Okamoto, Mechanical Systems Engineering*
"Passive Knee Assist Device for Squat Lifting: Toward High Usability" p.44

11:20 - 11:40 **Benye Tang** …*Advisor: Prof. Noritsugu Umehara, Micro-Nano Mechanical Science and Engineering*
"Friction Controlling Method with Optimal Solid Lubricant Conditions" p.47

11:40 – 11:55 Completion ceremony

12:00 – 13:00 Farewell lunch at Chez Jiroud (Closed)

Nagoya university JUACEP

052-789-2799 JUACEP Office

NAGOYA UNIVERSITY

Inserted Wedge-shaped CoFe Layer Studied by Time-Resolved Magneto-optical Kerr Effect (TR-MOKE)

Yu-Ching Hsiao
Mechanical and Aerospace Engineering, UCLA

Prof. Satoshi Iwata, Prof. Takeshi Kato, Prof. Daiki Oshima
Institute of Materials and Systems for Sustainability, Nagoya University

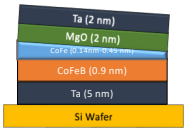

1

Motivation

- Memory Device

- High density
- High Speed
- Low power consumption

- Magneto-Resistive Random Access Memory (MRAM)

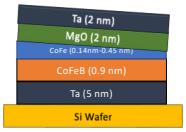

2

What is MRAM?

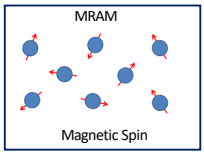

- Non-volatile

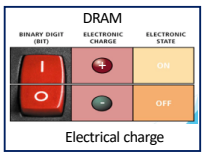

Logic 1

Logic 0

Logic 1

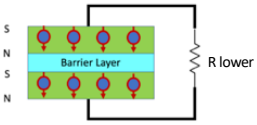

R lower

Logic 0

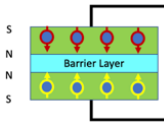

R Higher

3

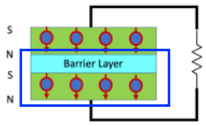

Project Goal: Reduce Energy Consumption

- Optimize damping coefficient
- Insert wedge-shaped CoFe to engineer anisotropy

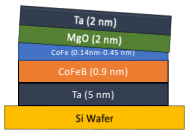

Magneto-optical spectroscopy
➢ Magnetization Easy Axis

TR-MOKE
➢ Damping Coefficient

4

Magnetization Easy Axis Change v.s Thickness

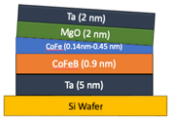

CoFe Thickness decreases

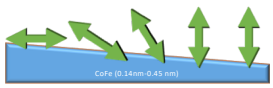

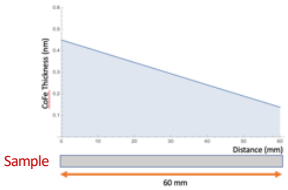

5

Magneto optical spectroscopy

➢ Hysteresis Loop

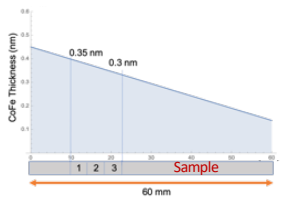

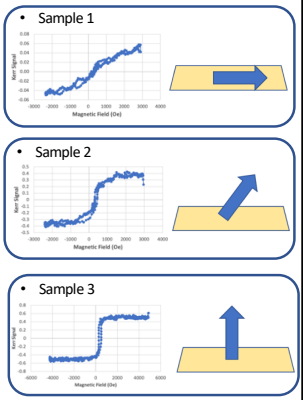

Magneto optical spectroscopy
➢ Hysteresis Loop

TR-MOKE
➢ Damping Coefficient

6

What is TR-MOKE?

- Pump Probe System

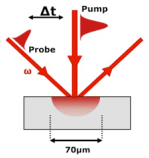

- Ultra-fast Dynamic Magnetization Switching 10-100 ps (10^{-12} second)
- Ultra-short pulse laser ~ 100 fs (10^{-15} second)
  - ➢ High magnetic resonance frequency (GHz)

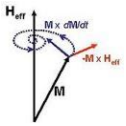

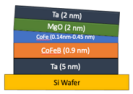

TR-MOKE

➢ 40 GHz

7

Experimental Set-up

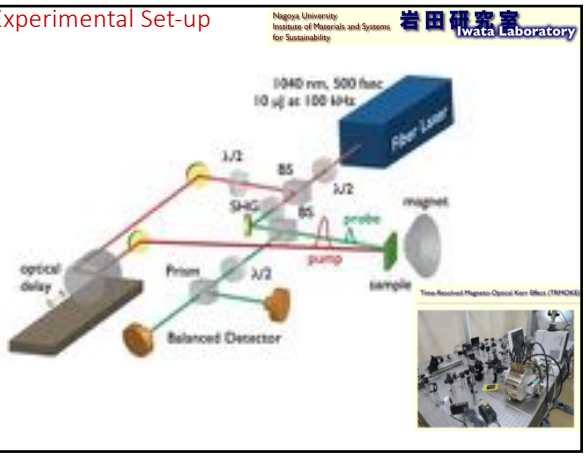

8

Pump-Probe System

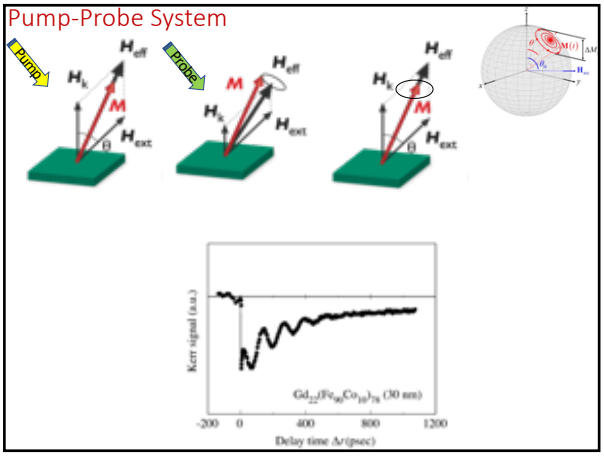

9

Results: Sample #1

- Vary External Field

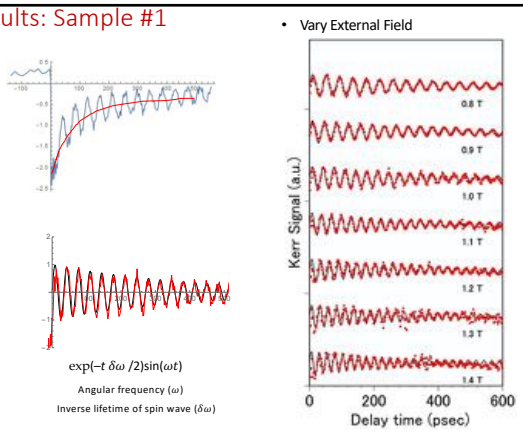

10

Results: Sample #1

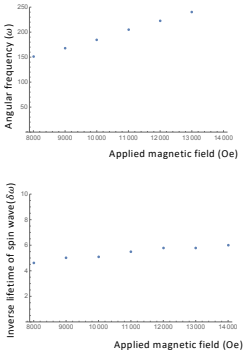

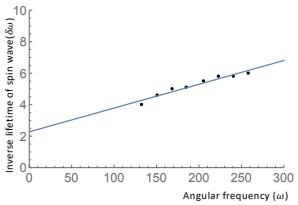

Damping Coefficient

$$\alpha = \frac{\delta\omega}{2\omega} = \frac{slope}{2} = 0.00755$$

11

Results

Sample	Thickness	Easy axis	Damping coefficient	g-factor	H_{keff} (Oe)
#1	0.35	IP	0.00755	2.05	-1800
#2	0.33	IP-OOP	0.00827	2.05	-500
#3	0.31	OOP	0.00947	2.05	500

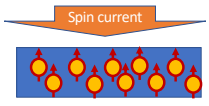

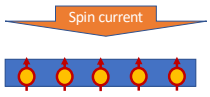

- Lower thickness → Easier to switch magnetization → Larger damping coefficient

As thickness decreases, damping coefficient increases

12

Conclusion

- In-plane to out-of-plane transition was observed

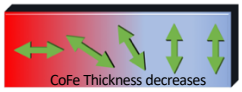

- Damping coefficient can be modified by inserted wedge-shaped layer CoFe
  As thickness decreases, damping coefficient increases

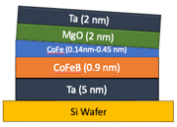

13

Acknowledgement

Nagoya University
Institute of Materials and Systems for Sustainability
岩田研究室
Iwata Laboratory

14

Effect of Different Orientations of Compensation Chamber on Loop Heat Pipe System for Automobiles

Guanru Feng
Supervisor: Prof. Hosei Nagano

University of Michigan
Mechanical Engineering
JUACEP Program
Thermal Control Engineering Group
08/30/2019

1

Presentation Outlines

- Introduction
- Design Model
- Experiment Results
- Conclusion and Future Works

2

Introduction

- Why LHP?
  - Environmental issue (60% heat wasted)
  - Long-distance transportation
  - High efficiency during transportation
  - Self-started, no other energy needed

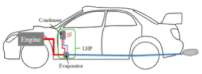

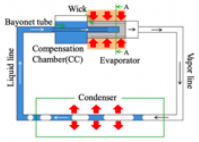

3

Thermodynamic Analysis

- P-T Diagram

1-2: Groove 2-3: Vapor line 3-6: Condenser
4-5: Vapor-liquid interface. 6-7: Liquid line
7-8: Compensation chamber
8-9-1: Evaporator

$$P_{cap} + \Delta P_g \geq \Delta P_{vl} + \Delta P_{ll} + \Delta P_{con} + \Delta P_{wick} + \Delta P_{gr}$$

$$P_{cap} = \frac{2\sigma \cos\theta}{r_{pore}}$$

σ: surface tension
Θ: liquid and pipe contact angle

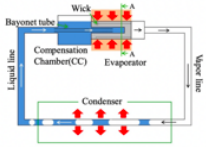

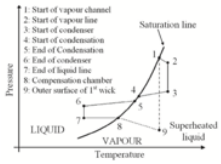

4

Components

1. Compensation Chamber
- Store excess working fluid
- Supply wick with working fluid
- Two phases coexist

$$V_v = (\rho_l V_{cc} - M_{cc})/(\rho_l - \rho_v)$$

$$V_l = (M_{cc} - \rho_v V_{cc})/(\rho_l - \rho_v)$$

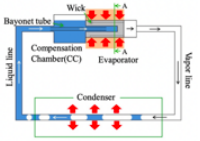

5

Components

2. Vapor, Liquid Line
- Simple pipes with insulation
- Single phase exists
- Frictional pressure loss

$$\frac{dP}{dL} = f \times \frac{\rho u^2}{2} \times \frac{4}{d_i}$$

$$f = \begin{cases} 16/Re, & Re < 2200 \\ 0.0791 \times Re^{-0.25}, & 2200 < Re < 10^5 \end{cases}$$

- Energy Conservation

$$-mC_p \frac{dT}{dL} = G_i \times (T_i - T_{amb})$$

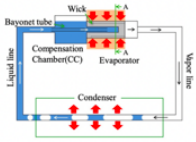

f: Frictional factor
ρ: Fluid density
u: Fluid velocity
d_i: Inner diameter
Re: Reynolds number
G: Thermal conductance

6

Components

3. Evaporator
- Vaporize working fluid
- Thermal energy from heat block

$$Q_{load} = G \times (T_{HB} - T_e)$$

  - Heat leak to CC
  - Evaporation
- 40 grooves in the evaporator
  - Pressure drop: same equation as simple pipe

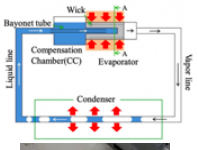

7

Components

4. Wick
- Porosity of 0.4 and pore size of 1.2μm radius
- Pressure change (Darcy's Law)

$$\Delta P_{wick} = \frac{m \times \mu \times \ln(\frac{r_o}{r_i})}{2\pi K_{wick} L_{wick}}$$

μ: Viscosity of fluid
K: Permeability of formation
L: Length

- Energy equation

$$Q = \frac{k_{eff} L_{wick} w_{wick}}{h_{wick}} \times \Delta T$$

$$k_{eff} = {k_{max}}^{0.42} \times {k_{min}}^{0.58}$$

$$k_{max} = \varepsilon k_l + (1 - \varepsilon) k_{wick}$$

$$k_{min} = \frac{k_l k_{wick}}{\varepsilon k_{wick} + (1 - \varepsilon) k_l}$$

ε: porosity

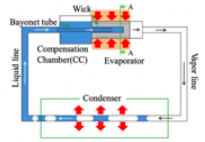

8

Components

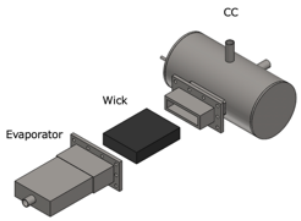

9

Components

5. Condenser
- Condensation
- Pressure change equation (Lockhart-Martinelli Equation)

$$\Phi_l^2 = \frac{\Delta P_{tp}}{\Delta P_l}$$

$$\begin{cases} \Phi_l^2 = 1 + cX + X^2 \\ \Phi_l^2 = 1 + \frac{c}{X} + \frac{1}{X^2} \end{cases}$$

$$c = \begin{cases} 5, \ if \ Re_l < 2300, Re_l < 2300 \\ 10, if \ Re_l < 2300, Re_l \geq 2300 \\ 12, if \ Re_l \geq 2300, Re_l < 2300 \\ 20, if \ Re_l \geq 2300, Re_l \geq 2300 \end{cases}$$

$$X = \frac{\Delta P_l}{\Delta P_v}$$

- Energy equation

$$\frac{dx}{dz} = \frac{1}{\dot{m}\lambda} G \Delta T$$

λ: latent heat of vaporization
x: vapor quality

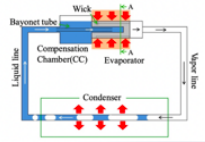

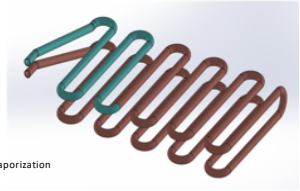

10

Components

6. Thermocouple
- Measure local temperature
- Average temperature
- Attached on whole LHP

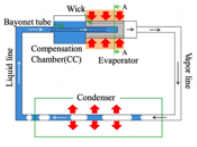

11

Components

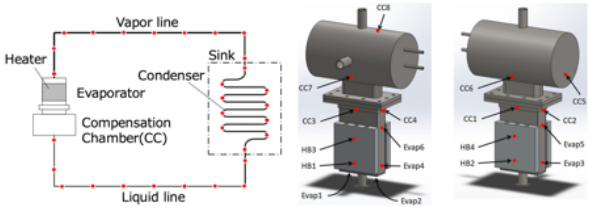

12

Components

All components geometric measurements

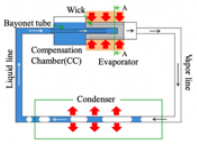

	Length	Width	Height
Heat Block	100	100	16
Evaporator	153	112	40
Wick	130	100	30
Groove	110	2.5	2.5
	Length	Inner Diameter	Outer Diameter
Condenser	5000	12.7	10.7
Vapor Line	2100	19.05	16.57
Liquid Line	2000	9.525	7.745

13

Experiment Results

- **Different Orientation of CC**
  - Vertical vs. Horizontal
- **Different Condenser Cooling Method**
  - Natural-Air Convection
  - Forced-Air Convection
  - Natural-Water Convection

14

Vertical vs. Horizontal

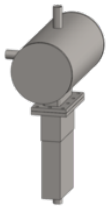

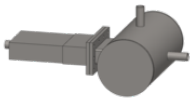

15

Experiment Results

- **Natural-air convection**
  - Condenser is exposed to ambient air directly
  - Only heat transfer due to temperature difference between condenser and ambient

16

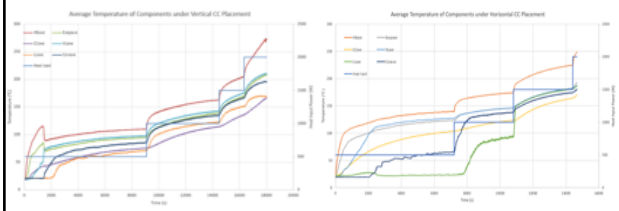

17

Experiment Results

- **Forced-air convection**
  - Fan and circulator will generate air flow to transfer heat

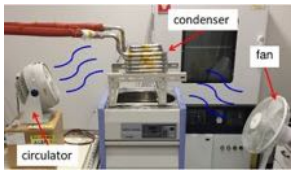

18

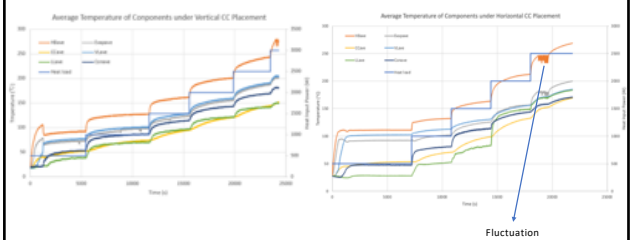

19

Experiment Results

- **Natural-water convection**
  - Condenser is fully immersed in a water tank full of water
  - Tank water temperature is ambient temperature

20

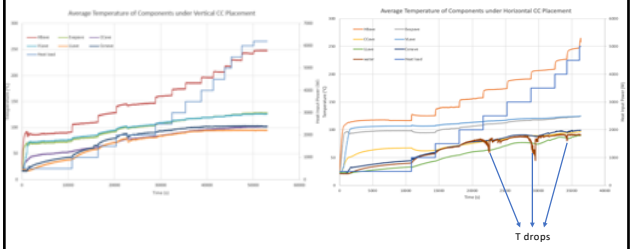

21

Experiment Results

- **Thermal Resistance Comparison**

$$R_t = \frac{\Delta T}{q}$$

  - Integrated system
  - Evaporator and condenser temperature difference
  - Heat input is from heat source
  - Heat output is from condenser

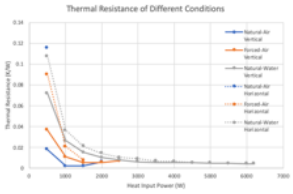

22

Conclusion and Future Works

- Vertical CC orientation with natural-water convection method shows the best performance when heat load is greater than 3000W
- Below 2000W, vertical CC orientation with natural-air convection is better
- Forced-water convection method will be tested
- Tilted CC orientation will be tested

23

Acknowledgement

I wish to acknowledge the support of the Japan-US-Canada Advanced Collaborative Education Program for the visiting graduate student opportunity. I wish to thank Professor Hosei Nagano and lab members of Thermal Control Engineering Group for the suggestions and advice during the research.

24

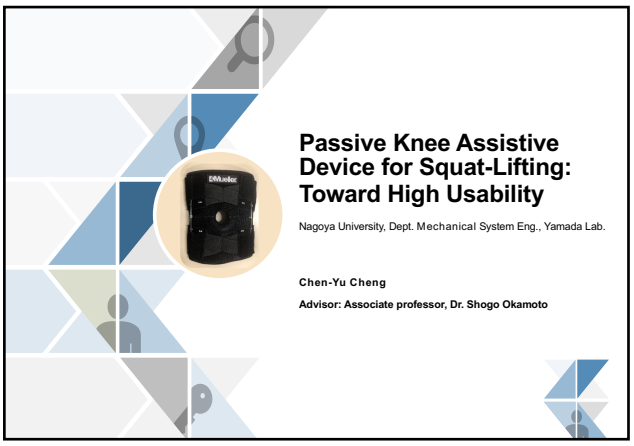
Passive Knee Assistive Device for Squat-Lifting: Toward High Usability
Nagoya University, Dept. Mechanical System Eng., Yamada Lab.
Chen-Yu Cheng
Advisor: Associate professor, Dr. Shogo Okamoto

1

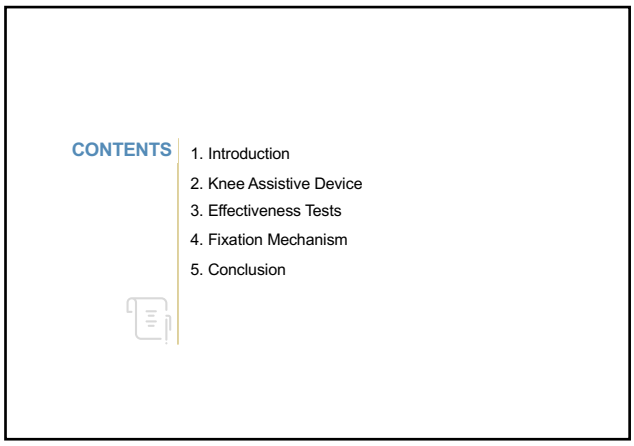
CONTENTS
1. Introduction
2. Knee Assistive Device
3. Effectiveness Tests
4. Fixation Mechanism
5. Conclusion

2

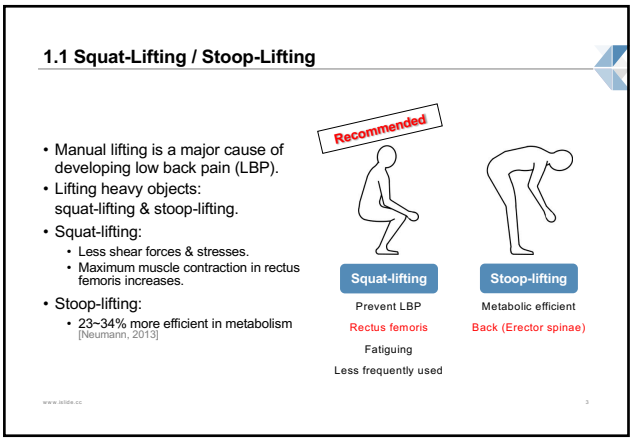
1.1 Squat-Lifting / Stoop-Lifting
• Manual lifting is a major cause of developing low back pain (LBP).
• Lifting heavy objects: squat-lifting & stoop-lifting.
• Squat-lifting:
• Less shear forces & stresses.
• Maximum muscle contraction in rectus femoris increases.
• Stoop-lifting:
• 23~34% more efficient in metabolism [Neumann, 2013]
Recommended
Squat-lifting
Prevent LBP
Rectus femoris
Fatiguing
Less frequently used
Stoop-lifting
Metabolic efficient
Back (Erector spinae)

3

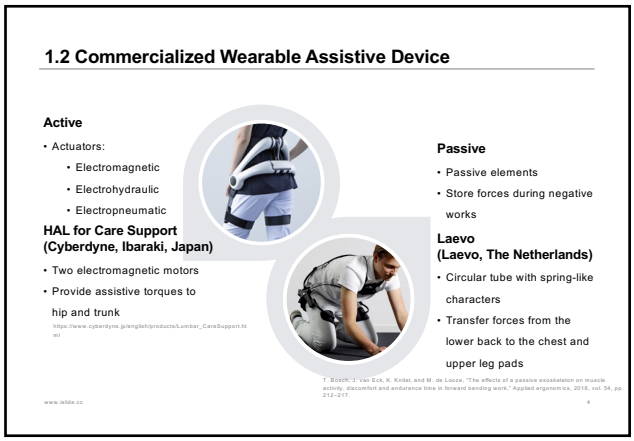
1.2 Commercialized Wearable Assistive Device
Active
• Actuators:
• Electromagnetic
• Electrohydraulic
• Electropneumatic
HAL for Care Support (Cyberdyne, Ibaraki, Japan)
• Two electromagnetic motors
• Provide assistive torques to hip and trunk
Passive
• Passive elements
• Store forces during negative works
Laevo (Laevo, The Netherlands)
• Circular tube with spring-like characters
• Transfer forces from the lower back to the chest and upper leg pads

4

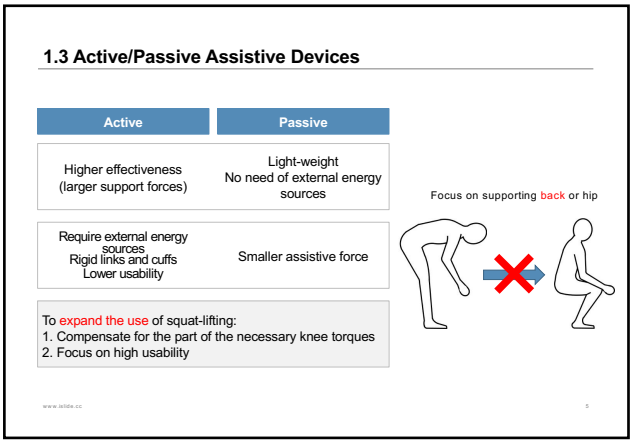
1.3 Active/Passive Assistive Devices
Active
Passive
Higher effectiveness (larger support forces)
Light-weight
No need of external energy sources
Require external energy sources
Rigid links and cuffs
Lower usability
Smaller assistive force
To expand the use of squat-lifting:
1. Compensate for the part of the necessary knee torques
2. Focus on high usability
Focus on supporting back or hip

5


2.1 Knee Brace
• Commercial hinged knee brace (54557, Mueller Sports Medicine Company)
• Original hinges were removed.
• Used as a soft chassis.
• Easy-to-wear: using two Velcro strips.

6

2.2 Shape-Memory-Alloy (SMA) Wires

- Nickel-titanium (Ni-Ti) alloy (Yoshimi Inc., Japan)
- Superelasticity (pseudoelasticity)
- Four wires were joined together
- Put in the pocket at each side of the knee brace.
- Designed specification: 10% of the required knee torques.
  - The maximum knee torque for sit-to-stand movement is 26.6 Nm for a 70-kg person (0.38 Nm/kg).

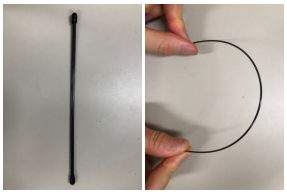

7

2.3 Determination of Diameter and Length of SMA Wires

- A push-pull scale (FB-100N, Imada Co. Ltd., Japan) was used.
- The push-pull scale was aligned with the direction of the restoring force of the wire.
- The resultant torque was measured at 100° (the maximum knee angle of a sit-to-stand motion).

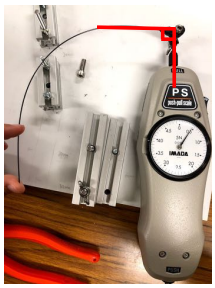

8

2.3 Determination of Diameter of SMA Wires

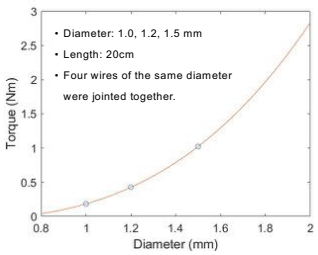

- Larger diameter wires generate greater torque.
- Nonlinear (quadratic)

9

2.3 Determination of Length of SMA Wires

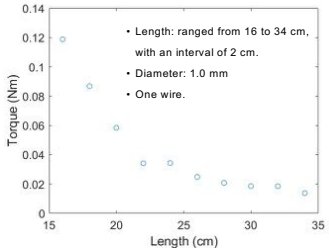

- Shorter wire generate greater torque.
- > 22 cm, the torque difference become smaller.

10

2.3 Diameter and Length of SMA Wires

- Length: 22 cm.
- Diameter: 1.8 mm.
- Number of wires: 8 (four wires per strand).
- This combination can produce 10% (2.66 Nm) of the required torque.

11

3.1 Experiment Procedure

- Measured the EMG signals of rectus femoris.
- Four conditions: 45° or 90°-squat with or without the knee assistive device.
- Pause for 5 seconds at the designed position.
- Each condition: 10 times in total.
- Tested in randomized order with each condition repeated 5 times a row.
- The participants didn't lift any objects.

3.2 Participants

- Three participants, height: 166.7 ± 9.1 cm, weight: 55.3 ± 5.9 kg.
- All participants were healthy with no injuries or diseases.

12

3.3 Data Analysis

- Focused on the central 3 seconds within the 5-second-pause.
- Calculate the mean voltage signal of each trial

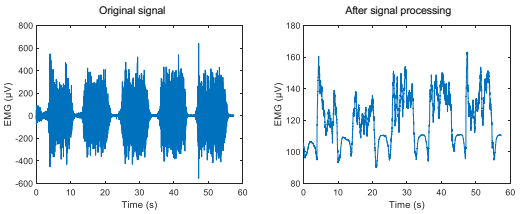

13

3.4 Results

- There is significant difference between with and without the knee assistive device. (Welch's *t*-test)
- 45°-squat: decreased by 27.7%.
- 90°-squat: decreased by 14.7%.

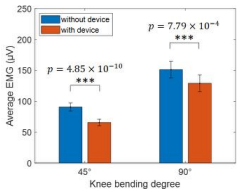

14

3.4 Results

- 45°-squat: decreased by 26.8%, 52.1%.
- 90°-squat: decreased by 22.9%, 38.4%.
- The different effectiveness may result from distinct weight and exercising habits.

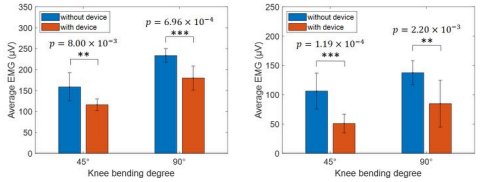

15

4 Fixation Mechanism

- Efficiently turn on and off the assistive torque.

Cylinder
- 2 square holes
- To confine horizontal movements

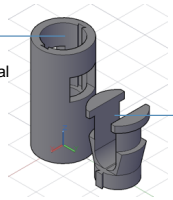

Lid with two "ears"
- 2 convex squares (fit into square holes)
- To confine vertical movements

16

4. Fixing Mechanism

17

5. Conclusion

- No previous device encourages squat-lifting
  - Passive knee assistive device (knee brace + 8 SMA wires) was proposed.
  - Support approximate 10% of the required torque.
- The EMG signals indicated that with the device, the activity of rectus femoris can decrease 14.7—52.1%.
  - The device is able to encourage people to change their lifting behavior.
- Future works
  - Evaluate practical utility (subjective feedback from occupational users).
  - With loads, the results would have be lower.

18

2019 JUACEP Summer Research

UMEHARA LABORATORY Tribo The Pursuit of Excellence

Friction Controlling Method with Optimal Solid Lubricant Conditions

Benye Tang

Integrative System + Design Department
University of Michigan

August 30th, 2019 Nagoya, Japan

Supervisors：Noritsugu Umehara, Takayuki Tokoroyama, Motoyuki Murashima

0

Background

- Satellite
  - About 10% of breakdown happened in sliding parts
  - Maintenance is impossible
- Wind turbine generator
  - High maintenance cost

Factors of breakdown
- Worn by abrasive powder
- Adhered by contamination

The condition of friction surface changes

Adapt to dynamic friction surface

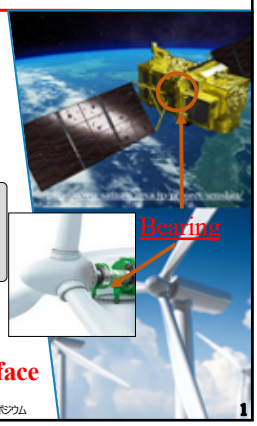

[1]加藤明，世界の人工衛星の不具合における自然環境の影響度，第31回宇宙環境シンポジウム

1

1

Previous research

- Proposal of smart surface[2]

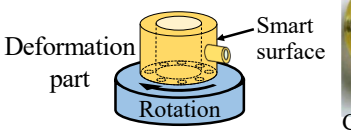

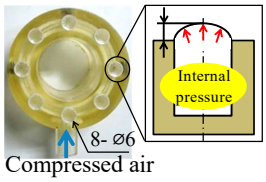

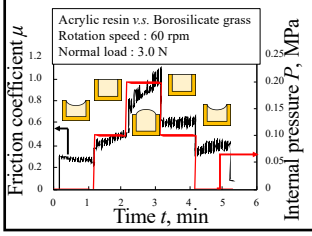

- Active friction control succeeded by changing the surface shape

Use the deformation mechanism

[2]M. Murashima, 'Intelligent tribological surfaces: from concept to realization using additive manufacturing', international Journal of Mechanical and Materials in Design, pp1-10, January 2019

2

2

Previous research

Developing a novel control method based on GA(*Genetic Algorithm*) which can adapt to the condition of counter surface

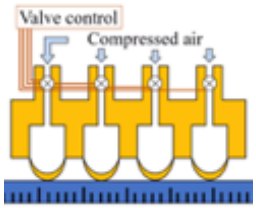

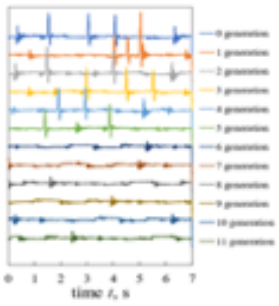

- Stable friction
- Long-life friction parts
- Lower maintenance cost
- Higher reliability

3

3

Purpose

Studying friction control method with solid lubricant conditions, and providing supportive reference for the application of GA

~Previous research~

Friction test on nylon plate with one damage part

For practical application in the future:

Good solid lubrication : MoS_2 & PTFE

~Current research~

The factors which affect stable friction are studied:

- The effect of # of contact points
- The effect of contact patterns
- The effect of thickness of coating film

The setting parameters for control method based on GA

4

4

Experimental apparatus & friction pair

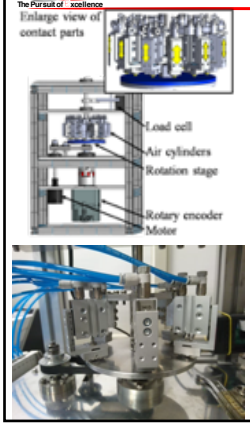

MC nylon coated by MoS_2 & PTFE
Size: Φ130 × 5 mm

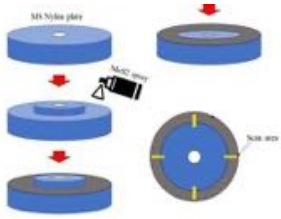

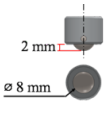

- High-carbon chromium bearing steel
- Ra = 10 nm
- HRC = 60

5

5

Experiment method

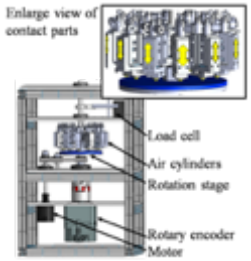

Transfer electrical signal to coefficient of friction

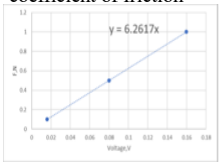

N	V
0.1	0.01597
0.5	0.079851
1	0.159701

load cell device constant $\alpha = 6.2617$

$$\mu = \frac{F[N]}{W[N]} \quad F = \alpha|V| \quad \Rightarrow \quad \mu = \frac{\alpha|V|}{W[N]}$$

Experiment conditions:
Load: W = 13.4 N
Rotation speed: v = 40 rpm
Test duration: t = 3600 ~ 14400 sec

6

6

Experimental result: # contact points

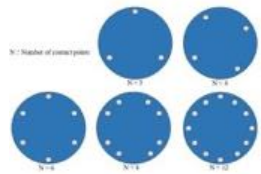

Amplitude of CoF = $CoF_{max} - CoF_{min}$

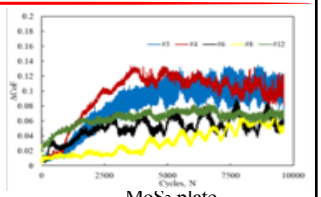

MoS_2 plate

6 and # 8
Smaller fluctuation of ΔCoF

3 and # 4
Bigger fluctuation of ΔCoF

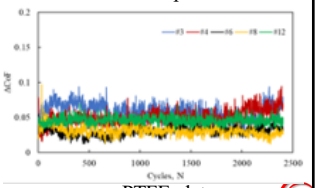

PTFE plate

7

7

Discussion: # contact points

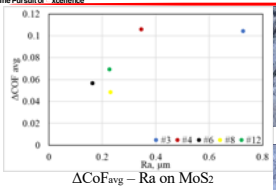

ΔCoF_{avg} – Ra on MoS_2

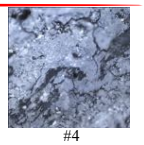

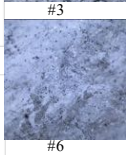

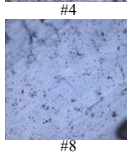

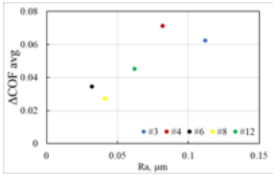

ΔCoF_{avg} – Ra on PTFE

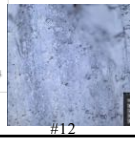

- Roughness is the significant factor
- The fewer number of contact points should be considered carefully

8

8

Experimental result : contact patterns

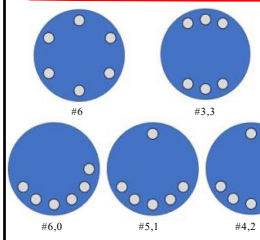

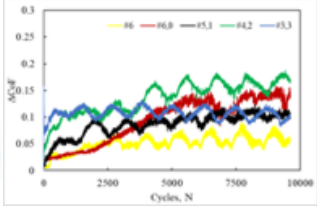

- Symmetrical patterns show the better performance
- The plates of unsymmetrical patterns were tested under unstable friction
- The unsymmetrical patterns should be treated carefully before setting the initial conditions of GA program

9

9

Experimental result: thickness of film

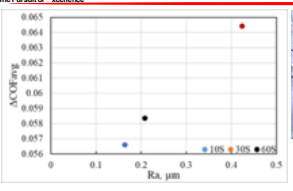

The different thickness of coating films

spray time(sec)	Film thickness(㎛)	Wear track depth(㎛)	Remained thickness(㎛)
10s	54.9	25.4	29.5
30s	94.8	56.5	38.3
60s	130	118	12.3

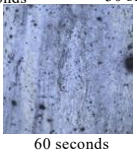

Test plates: 10 seconds' coating
30 seconds' coating
60 seconds' coating

- Roughness is a significant factor
- The thicker the coating, the lower the adhesion energy is, then the easier it is stripped

10

10

Conclusions

- Roughness is a significant factor, which affects the amplitude of coefficient of friction significantly
- The fewer number of contact points should be treated carefully, which can result in the cracks on the surface because of the higher contact pressure
- Symmetrical patterns have the advantage over the unsymmetrical patterns
- The MoS_2 coating film is not the thicker, the better. And its relation with surface roughness should be further studied.

11

11

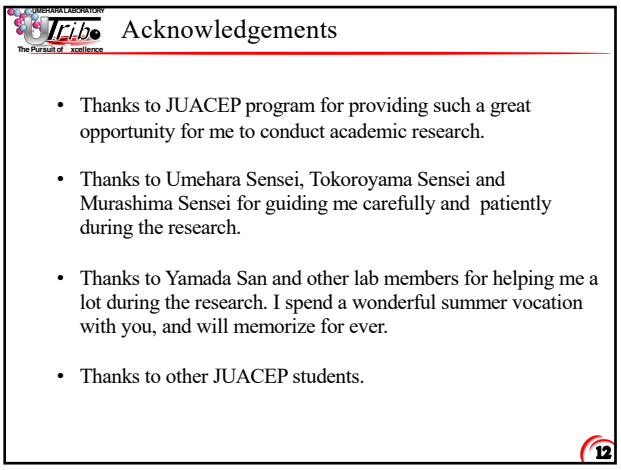
UMEHARA LABORATORY
Tribo
The Pursuit of Xcellence
Acknowledgements
• Thanks to JUACEP program for providing such a great opportunity for me to conduct academic research.
• Thanks to Umehara Sensei, Tokoroyama Sensei and Murashima Sensei for guiding me carefully and patiently during the research.
• Thanks to Yamada San and other lab members for helping me a lot during the research. I spend a wonderful summer vocation with you, and will memorize for ever.
• Thanks to other JUACEP students.
12

12

<3> Classes and Events

(a) JUACEP Summer Program 2019 Japanese Course Syllabus

Course name	Japanese Language
Teaching staff	Ms. YASUI Sumie
Course period	June 19 - July 23, 2019
Weekly timetable	Tuesday 3rd (45 min) & 4th period (90 min) 13:45-16:15 Wednesday 1st (45 min) & 2nd period (90 min) 9:30-12:00
Classroom	Seminar Room B of Nagoya University Library 2nd floor
Textbook	"GENKI An Integrated Course in Elementary Japanese" I (The Japan Times) This textbook is a comprehensive approach to developing the four basic language skills (listening, speaking, reading and writing) in order to cultivate overall Japanese-language ability. *Some teaching material will be given in class.
Course Contents	**Course outline** The purpose of this course is to introduce the most essential Japanese words and expressions for everyday life. Students will learn writing system (Hiragana & Katakana), the basic grammar, expressions of Japanese. **Classroom activities** Basic communication skills required in everyday life will be taught by introducing new vocabulary, new grammar, and practicing listening, conversation and role-playings. **Homework and Quiz** You are expected to submit your homework by the deadline. Quizzes will be given every day in class. 1. Hiragana 2. Katakana 3. Dictation 4. Conjugation
Evaluation	1. Homework 20% S=100-90 2. Quizzes 30% A=89-80 3. Oral exam. 50% B=79-70 100% C=69-60 More than 80% attendance is required. F(fail)=59-0 You will be officially awarded 1 credit of Nagoya University.

Course schedule	1. 6/19 (Wed) Greeting Expressions, Hiragana 1 Introducing yourself , Noun sentences 1, Occupation, Nationality, Age, Numbers 1-100 2. 6/25 (Tue) Classroom expressions, Hiragana 2 Shopping, Noun sentences 2, Price, Numbers 101-1,000,000 3. 6/26 (Wed) Hiragana 3 Describing where things are, Locations Placing an order at a restaurant 4. 7/2 (Tue) Hiragana 4 Talking about your daily life Verbal sentences 1, Time reference, Adverbs 5. 7/3 (Wed) Hiragana 5 Invitations, Suggestions, Desires Verbal sentences 2, Days/Weeks/Months/Years, Counting 6. 7/9 (Tue) Katakana 1 Talking about your family Adjectives, Likes or Dislikes, Degree expressions, Family terms 7. 7/10 (Wed) Katakana 2 Talking about your week-end, Past tense, Time words 8. 7/16 (Tue) Katakana 3 Making a request (Verb-Te-form), Progressive actions, Describing your status 9. 7/17 (Wed) Asking permission, Prohibition, Negative request Describing two things Talking about your interests Plain form 10. 7/23 (Tue) **The Final Examination (speaking)**

(b) Hands-on Exercise

"Disassembly and Assembly of Internal Combustion Engine"

Date: 13:00 – 16:30, July 4th, 2019

Place: Creation Plaza, 10th floor of IB-North

Staff: Prof. Tsuyoshi Inoue, Director of Creation Plaza
Technical staff… Nakakimura, Goto, Saito, Isogai, Adachi and Yamamoto
Teaching Assistants… Yumena Iki, Ruixi Zhang, Wangzhen Zhao, Yuki Akizuki, Yoshitada Aono

Contents:

1. Opening remarks
2. Introduction to the basis of the Internal Combustion Engine and other engines
   (History, Characteristics, Operation principle, Demonstration of engines)
3. Disassembling → Assembling → Adjustment
4. Performance test
5. Jet engine demonstration
6. Discussion, questionnaire

(c) Excursion

Date: July 5, 2019

Fee: 2,000 yen

Visiting spots:

・Toyota Kaikan Museum
http://www.toyota.co.jp/en/about_toyota/facility/toyota_kaikan/museum/

・Toyota Motor Factory
http://www.toyota.co.jp/en/about_toyota/facility/toyota_kaikan/index.html

・Asahi Brewery Nagoya
https://www.asahibeer.co.jp/brewery/language/english/#Nagoya

・Tokugawa Museum
https://www.tokugawa-art-museum.jp

・Dinner at Nagoya station area

Schedule:

Time	Event	Transportation
9:00	Meeting at Toyoda Auditorium	
9:10	Departure from Nagoya University	Hired bus
10:00	Toyota Kaikan Museum	
10:30	Toyota Factory Tour	
13:00	Leaving Toyota and Lunch in the bus	Hired bus
14:00	Asahi Brewery Nagoya Tour	
15:10	Leaving Asahi Brewery	Hired bus
15:30	Tokugawa Museum	
17:00	Leaving Tokugawa Museum	Hired bus
18:00	Dinner	
19:30	Adjournment	Subway

*Schedule above is tentative and may be changed.
*Wear sports shoes for safety of the factory tour.
*Photo is not allowed in the factory.

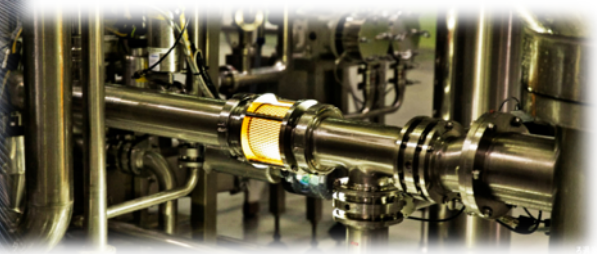

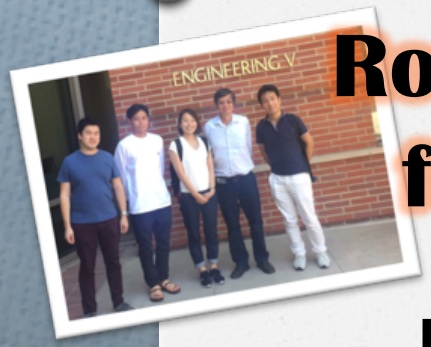

Round-Table Discussion for JUACEP Students

14:45 Thu, July 25, 2019

Lecture room#221 2F EB-2N

A Meet-up to get info for the life of study abroad!

- To reduce anxieties of your life abroad
- To know what you need for the beginning of your life abroad
- To have dependable friends in your life abroad....

Inquiry → JUACEP-OFFICE@engg.nagoya-u.ac.jp
phone 052-789-2799 (内線2799/4553)

(c) The 51st JUACEP Seminar

The 51st JUACEP Seminar

第 51 回名古屋大学日米加協働教育プログラムセミナー

13:30-14:30, Thursday, July 25, 2019
Lecture room 221 (2F, Eng.Bldg. II)

Miniaturized Gas Chromatograph Technology

Prof. Katsuo Kurabayashi

Department of Mechanical Engineering
Department of Electrical Engineering
and Computer Science
University of Michigan, U.S.A.

Abstract

Gas Chromatography (GC) is a powerful technique used in analytical chemistry for separating and detecting various vaporized compounds, such as volatile organic compounds (VOCs). Our modern society has seen a growing concern about human exposure to VOCs in the air that may cause potential health risks. The on-site continuous monitoring and point-of-care detection of these compounds enables accurate environmental health risk assessment and the rapid, non-invasive, early-stage screening of human diseases. However, conventional thermal modulator devices are resource-intensive, occupy a large instrument space, and /or demand a large amount of power for their operation. This talk describes our research efforts to develop key microelectromechanical systems (MEMS) devices necessary for realizing miniaturized low-power, low-cost, robust GC systems.

Biography

Katsuo Kurabayashi is Professor of Mechanical Engineering and Electrical Engineering and Computer Science at the University of Michigan, Ann Arbor. He received his BS in Precision Engineering from the University of Tokyo in 1992, and his MS and PhD in Materials Science and Engineering from Stanford University, CA, in 1994 and 1998, respectively. His current research focuses on optofluidics, nanoplasmonic and biomolecular biosensing, and BioMEMS/microsystems for immunology, clinical diagnosis, and analytical chemistry. He received the 2001 NSF Early Faculty Career Development (CAREER) Award, and the Robert Caddell Memorial Award in 2005, the Pi Tau Sigma Outstanding Professor Award in 2007, the Mechanical Engineering Outstanding Achievement Award in 2013 from the University of Michigan, and the Ted Kennedy Family Team Excellence Award in 2015 from the College of Engineering at the University of Michigan.

Inquiry: JUACEP Office 日米加協働教育プログラム (Ext. 2799)
JUACEP: Japan-US-Canada Advanced Collaborative Education Program, Graduate School of Engineering

<4> Feedback and Questionnaires

(a) Findings through JUACEP

Findings through JUACEP

Name: Benye Tang
Affiliation at home country: ISD Department, University of Michigan
Participated program: Summer Course 2019
Research theme:
Friction Controlling Method with Optimal Solid Lubricant Conditions
Advisor at Nagoya Univ: Prof. Noritsugu Umehara
Affiliation at Nagoya Univ.: Micro-Nano Mechanical Science and Engineering

This summer, I am very happy to participate in this JUACEP program at Nagoya University. Not only I conducted a research about tribology, but also achieved many things which can be written on my accomplishment list during this summer vocation.

It was my first time to get into Toyota plant to visit its production line which impressed me a lot. Toyota Production System is so famous, especially its lean manufacturing. When I was reading the book The Toyota Way, the seed of being able to visit Toyota production line one day was buried in my heart. I appreciate JUACEP office and Kato-san for organizing such a great excursion for us.

It was my first time to learn Japanese, and Yasui Sensei helped me a lot patiently. From those classes, I learned some basic knowledge of Japanese, such as Hiragana, greetings and some grammar. Even though learning a foreign language needs a lot of memory, I still find it is interesting because of Yasui Sensei's lively teaching. I hope to keep on learning Japanese after going back to United States.

It was my first time to travel around Japan. I went to Kyoto, Osaka, Tokyo, Sendai and Nagano, which made me learn more about Japanese society and its wonderful culture. And the summer trip organized by Umehara Lab is another unforgettable experience. We went to Lake Suwa in Nagano and lived in a cottage. The BBQ and blue berries picking organized by lab members were a lot of fun.

Time flies with joy all around! It's time to farewell to Nagoya University, to my respectful professors, to helpful JUACEP members, and to my friendly lab members. I will miss the ten weeks and the lovely people here forever. Hope to meet with these old friends again!

Findings through JUACEP

Name: Chen-Yu Cheng
Affiliation at home country:
Mechanical Engineering, University of Michigan – Ann Arbor
Participated program: Summer Course 2019
Research theme:
Passive Knee Assist Device for Squat Lifting: Toward High Usability
Advisor at Nagoya Univ: Prof. Shogo Okamoto
Affiliation at Nagoya Univ.: Mechanical Systems Engineering

It was an unforgettable experience this summer, not only did I learn more about the multidiscipline between human and engineering, improved my academic research abilities, but I also experienced lots of Japanese culture, including working attitude, eating habits, and understood more about the career in Japan, especially for women

Actually, I didn't have much independent research experience before I came here. Besides, although the research topic was interesting to me, I wasn't familiar with it. Hence, I faced difficulties at the first several weeks. Thanks to my advisor, Professor Okamoto, he offered me a lot of help, discussed the research progress with me very often. Also thanks to my lab mates, they taught me how to use the devices to do the experiments and also the method of signal processing.

Besides the research here, I'm interested in the careers in Japan, too. Hence, I talked to a student studied in Nagoya University who was doing an internship in Toyota during summer vacation. It was surprising to know that the working hours for an engineer were not as long as I expected, there was even a rule for not working overtime on Wednesday and Friday. I also talked with a woman who has been worked in Japan for 4 years as a sales assistant. The promotion for women are still worse than men in Japan, same as what I heard, but this situation has become better and better. Furthermore, because of the huge population of Chinese people nowadays, there are about 1/3 Chinese in her company, which make the culture of the company more similar to a mixture of Japanese and Chinese culture. Understanding these change in careers in Japan makes me more willing to look for a job here.

During the 10-week program, I spend several weekends to travel around Japan and experience the cultures here. Other than the architectures and weather here, I think the most different thing between Taiwan and Japan, or American and Japan, is the reactions between people. Japanese people tend to be very considerate, they are really good at reading the air, and helping others before they say their needs. However, this is both an advantage and a disadvantage: people seldom get disturbed in public places, but it will be tiring if you need to care about others all the time. But I think this is an important skill for me to learn from Japanese. Another interesting thing is that Japanese people are modest. Thus, if I tell them that I can only speak a little Japanese, they would regard me as being modest and talk to me in Japanese.

It was really a joyful and unforgettable experience for staying in Nagoya this summer. Not only did I gain experience on academic research, but I also enjoy Japanese cultures here. I will definitely come to Nagoya or other places in Japan again in the future. In general, JUACEP program is an amazing program that I'll recommends others to participant.

Findings through JUACEP

Name: Guanru Feng
Affiliation at home country: Mechanical Engineering, University of Michigan
Participated program: Summer Course 2019
Research theme:
Effect of Different Orientations of Compensation Chamber on Loop Heat Pipe System for Automobiles
Advisor at Nagoya Univ: Prof. Hosei Nagano
Affiliation at Nagoya Univ. :
Thermal Control Engineering Group, Mechanical System Engineering

Nagoya is a pretty and quiet city. It is a good place for study and research. The lab facilities and campus facilities are great. The ergonomics here in Japan is the best in my opinion. Everything here is designed for the convenience and safety of people. The garbage sorting really makes me confused at first, but later on I find out it's really efficient and friendly to the environment. The field trip to the Toyota Museum and Asahi Beer Factory really open my eyes. I gain a deeper knowledge on the front-field technologies in automotive industry and the producing process of beer. The engine assembly workshop is also fascinating. Although I'm focusing my career on the internal combustion engine, this is still my first time to get a hand-on experience outside classroom. I also visited Tokyo during weekend. It's a great city full of opportunities as well as fun. While Kyoto, on the contrary, is a city full of historic buildings. In Japan, I felt both the beauty of modern city and historic city.

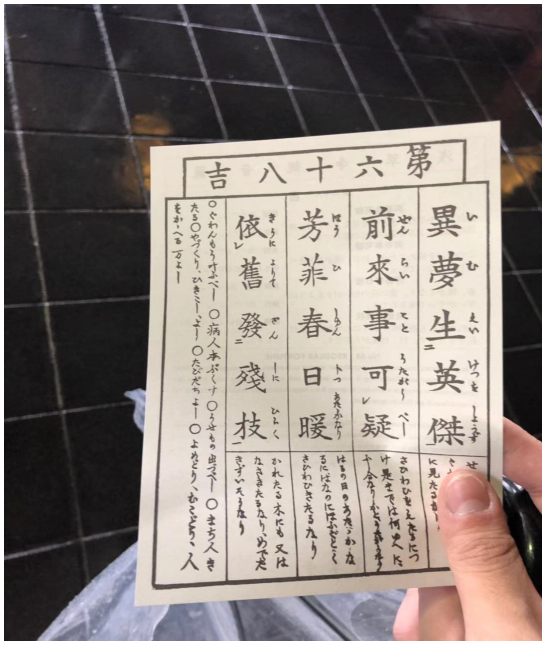

Findings through JUACEP

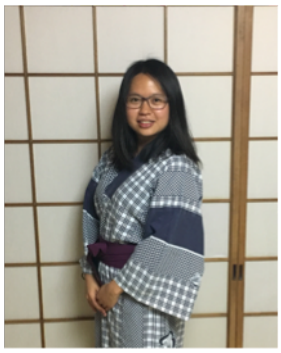

Name: Yu-Ching Hsiao

Affiliation: Mechanical and Aerospace Engineering, UCLA
Participated program: Summer Course 2019
Research theme:
Inserted Wedge-shaped CoFe Layer Studied by Time-Resolved Magneto-optical Kerr Effect (TR-MOKE)
Advisor at Nagoya Univ:
Prof. Satoshi Iwata, Prof. Takeshi Kato, Prof. Daiki Oshima
Affiliation at Nagoya Univ.: Institute of Materials and Systems for Sustainability

Before coming to Japan, I was very looking forward to the research opportunity and life experience here. Now I would say, "It did not disappoint me at all. I really enjoy it!"

I joined Prof. Iwata's lab this summer and chose the complicated equipment TR-MOKE as my research topic. Prof. Kato patiently walked me through all complex procedures step by step. Prof. Iwata and Prof. Oshima were very helpful when I encountered problems. The discussions with professors provoked my thoughts and deepen my understanding on my research magnetic dynamics. I greatly appreciate my research experience of operating TR-MOKE. I am excited to bring the newly gained knowledge and skills back with me to the U.S. to continue my journey as a better prepared doctoral student.

To all lovely lab members: due to my poor Japanese, in the beginning it was hard for me to communicate with them. I am very thankful they started teaching me Japanese. Day by day we overcame the language barrier and got to know each other better. In August, I was invited to the lab trip. Wearing yukata while having traditional Japanese food and playing with you guys are the highlights of my stay here. You guys make me like Japan much more!

Last but not least, I would like to express my gratitude to Tomoko-san. She always supports us whenever we need her. Without her, our lives here would be much more difficult. I remembered one evening I ran into her on campus. It was not her working hours but she still invited me for dinner and chat with me to make sure we were all doing fine. Thank you Tomoko-san. You make this program different.

Participating in JUACEP program is one of the best decisions I have made. Time flies. Good time makes leaving here hard. I will take the unforgettable memory with me back to the U.S. Love you all!

(b) Questionnaires

For Q1-4, we asked the same questions BEFORE and AFTER the program.

Q.1: Are you interested in studying at a Japanese university for PhD?

Before

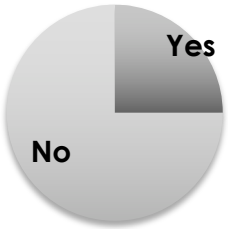

After

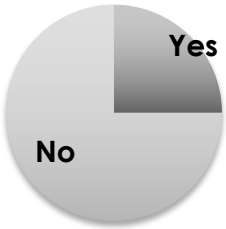

Q.2: Are you interested in working at a Japanese company in USA?

Before

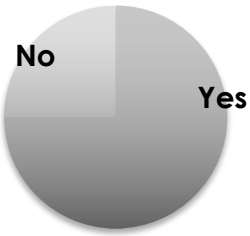

After

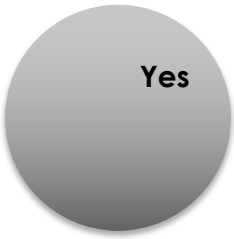

Q.3: Are you interested in working at a Japanese company in Japan?

Before

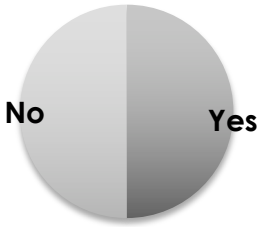

After

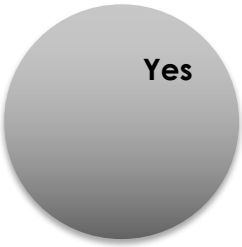

Q.4: Are you interested in working at a non-Japanese company in Japan?

Before

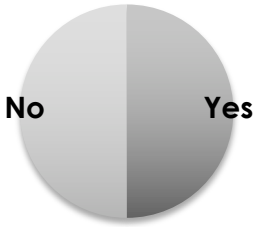

After

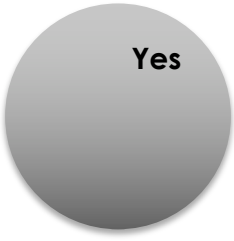

Q.5: Which activity did you like? ('Research internship', 'Field trip', 'Engine assembly', 'Japanese course', others)

All students answered they liked every activity they participated.

Q.6: In what did you find difficulty? What could be improved? (Excerpts)

- Because of the language barrier, sometimes it is hard for me and my lab members to understand well, especially when we discuss about the research or conduct experiment.

- I would recommend to offer advanced Japanese courses so that we can improve our language skills more during the stay here.

- Just an idea: hold an event to gather all the international exchange students from different programs.

- Language is the most difficult part. I learnt Japanese before, but it's still very hard to catch up with the speed when people are speaking Japanese.

- If there is some career advice, it'll be greater.

Q.7: Write comments freely.

- I like Japan very much. Everything here is great. People are really nice and polite. I definitely want to come back again either for higher education or for work.

-Thanks a lot for every staffs, professors in both Nagoya University and University of Michigan.

It is a good program. Professors and JUACEP members in Nagoya University are very friendly and helpful.

<5> Appendices

(a) Photo Collection

June 18: Orientation & first meeting with lab members

Welcome address from Dean Prof. Mizutani

July 4: Hands-on exercise 'Internal Combustion Engine'

Engine lecture by TAs

Demonstration of stirling engines

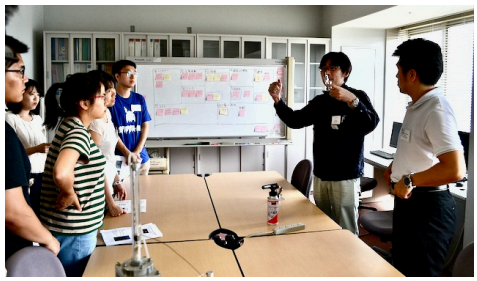

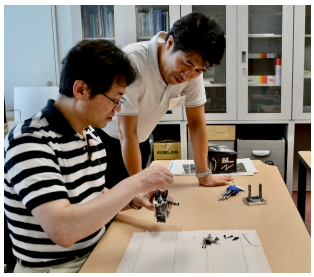

Disassembly/assembly of the engine model

Performance test

Demonstration
of the Jet engine

University dormitory ‘Residence Yamate South’

July 5: Field Trip

Toyota Kaikan Museum

Asahi Brewery

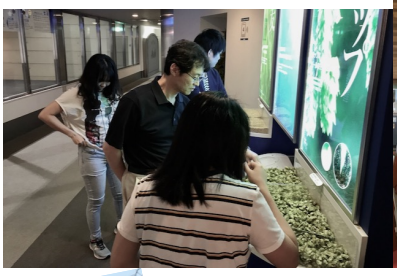

Tokugawa Museum

July 25: Seminar by Prof. Kurabayashi

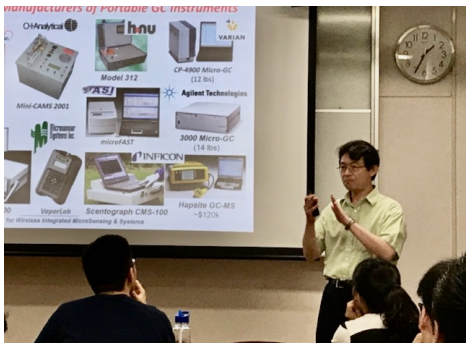

August 8: The 25th Workshop

Achievement presentations and discussions

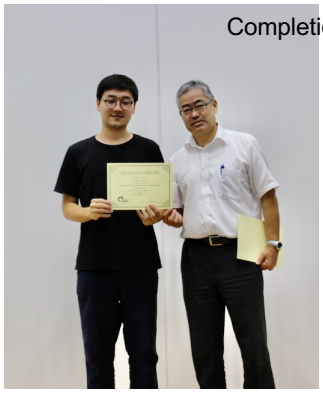

Completion ceremony

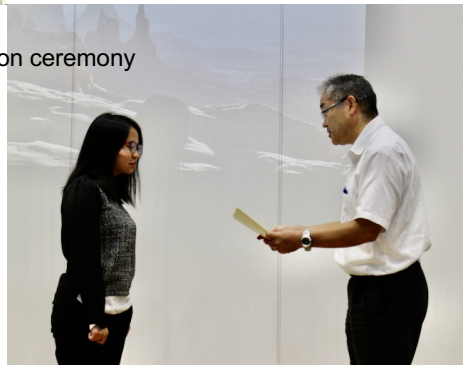

Farewell party at Chez Jiroud

(b) Building Location

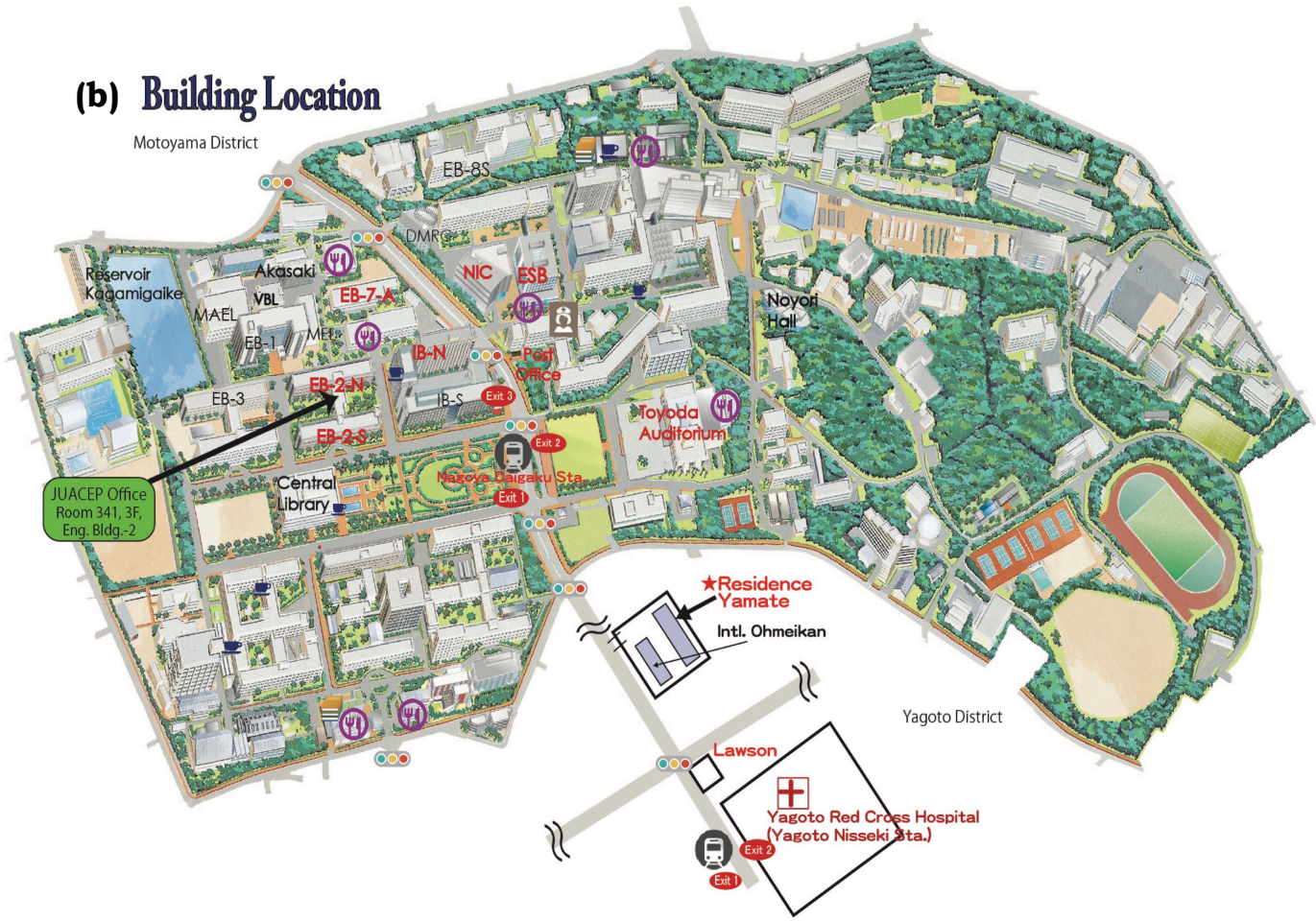

Bldg. icon on the map	Building name (in Japanese)	Important places for JUACEP	Lab locations for JUACEP students
EB-2N	Engineering Building 2 (Kougakubu ni-gou-kan, Kita)	JUACEP Office, Rm.341, 3F	Yamada Lab, 3F for Chen-Yu Nagano Lab, 4F for Guanru
EB-2S	Engineering Building 2 (Kougakubu ni-gou-kan, Minami)	Meet-up, July 9 at Rm.347, 3F	
EB-7A	Engineering Building 7 (Kougakubu nana-gou-kan, A)		Umehara Lab for Benye
IB-N	Integrated Building North (I-B, Kita)	Hands-on Exercise, 13:00-16:30, July 4 at Creation Plaza, 10F	Iwata Lab, 3F for Yu-Chin
ESB	Engineering & Science Building (E-S kan)	Orientation, Jun. 18 at ES Meeting Rm, 1F Stipend, 13:00, Jul. 3 & Aug. 2, 3F	
NIC	National Innovation Complex (Nic)	25nd Workshop, Aug. 30 at Idea Stoa, 1F	
Central Library		Japanese class at Seminar Rm B, 2F 13:45-16:15 for Tue. and 9:30-12:00 for Wed.	
Toyoda Auditorium	(Toyoda koudou)	Meeting point for Excursion, 9:00, Jul. 5	
Gymnasium			
Post Office		Money change, Money withdrawal, Postal affairs	
	Cafeteria/Convenience Shop		
	Café		
	Book Store		
	Subway Station	Nagoya Univ.: NagoyaDaigaku Station Dormitory Yamate: Yagoto Nisseki Station	
	Health Administration Office	Open hours: 9:00-12:00, 13:00-17:00, Mon.-Fri. (052)789-3970	

(c) Mandatory Deliverables

★ All of following templates can be downloadable at
http://www.juacep.engg.nagoya-u.ac.jp/downloads/index.html

1. JUACEP Independent research report
See *Appendix-1.*
Deadline: **August 28, 2019**
Send to… juacep-office@engg.nagoya-u.ac.jp

2. JUACEP Research presentation slides
We will collect your PowerPoint/PDF slides at the workshop site, **August 30, 2019**.

Evaluation: your final score is calculated by the points of the research report and the presentation at the workshop evaluated by your Nagoya Supervisor;

Research report (1~50pts.) + Presentation (1~50pts.)
100~90=S, 89~80=A, 79~70=B, 69~60=C, 59~0= fail

You will be officially awarded credits of Nagoya University and the transcript is airmailed to your home university in September 2019.

Important:
(a) JUACEP will publish the participants' research reports and the presentation slides in the website and booklet. Please let us know if your supervisor permits its publication by August 28.
(b) UM students MUST transfer the credits to ME590/Engr591 and submit the transcript to JUACEP Office as soon as possible.

3. Findings through JUACEP
See *Appendix-2.*
Deadline: **August 25, 2019**
Send to… juacep-office@engg.nagoya-u.ac.jp
Please write freely about your experience in Japan inserting pictures.

4. JASSO Scholarship obligatory questionnaires, H-1
See *Appendix-3.* There are "Pre-arrival" part which you already submitted and "After the program" part which you have to submit until **August 25, 2019.**
Send to… juacep-office@engg.nagoya-u.ac.jp

Published in December 2019

Japan-US-Canada Advanced Collaborative Education Program (JUACEP)
Graduate School of Engineering
Nagoya University
Furo-cho, Chikusa-ku, Nagoya 464-8603, Japan
JUACEP@engg.nagoya-u.ac.jp
http://www.juacep.engg.nagoya-u.ac.jp